# Signaling pathways and endogenous stem cell proliferation in *Tribolium castaneum*

by

William Tank

B.A., ESPM, 2004
B.S., Kansas State University, 2021

AN ABSTRACT OF A DISSERTATION

submitted in partial fulfillment of the requirements for the degree

DOCTOR OF PHILOSOPHY

Department of Biology
College of Arts and Sciences

KANSAS STATE UNIVERSITY
Manhattan, Kansas

2026

# Abstract

Endogenous stem cells are responsible for tissue maintenance, remodeling, and repair in many organisms. This project explored whether signaling pathways associated with proliferation and apoptosis could be manipulated to alter endogenous stem cell activity during post-embryonic development, with long-term interest in how these mechanisms could eventually contribute to regenerative approaches. Initial pathway comparisons examined Wnt, Notch, TGF-β, and Hippo signaling. The Hippo pathway was selected for further investigation because of its direct involvement in regulation of proliferation, apoptosis, and tissue growth. *Tribolium castaneum* was chosen as the experimental model because its midgut contains accessible intestinal stem cell clusters (nidi) and supports strong systemic RNA interference (RNAi).

Double-stranded RNA targeting Hippo pathway components including *hippo (hpo)*, *warts (wts)*, *yorkie (yki)*, and *salvador (sav)* was injected into larval, pupal, and adult stages. Midgut tissues were evaluated using EdU incorporation assays, fluorescence microscopy, histology, RT-qPCR, and RNASeq. Among the genes tested, *salvador* knockdown produced the strongest and most consistent phenotype. Midgut tissues displayed disrupted epithelial organization, widespread EdU incorporation, nuclear crowding, tissue fragility, and abnormal nidi morphology across developmental stages. Similar abnormalities were reproduced using an independent *salvador* dsRNA construct. RT-qPCR confirmed reduction of *salvador* transcript expression following RNAi treatment.

RNASeq analysis following *salvador* knockdown identified transcriptional changes associated with epithelial organization, ion transport, stress responses, and cytoskeletal regulation rather than a clear enrichment of canonical proliferative signatures. The observed

phenotype was therefore interpreted as dysregulated proliferative activity associated with loss of epithelial organization rather than controlled regenerative expansion.

This work supports the use of *Tribolium castaneum* as a model for studying Hippo pathway function during post-embryonic intestinal remodeling and demonstrates that disruption of *salvador* produces extensive abnormalities in proliferative regulation and midgut organization.

# Signaling pathways and endogenous stem cell proliferation in *Tribolium castaneum*

by

William Tank

B.A., ESPM, 2004
B.S., Kansas State University, 2021

A DISSERTATION

submitted in partial fulfillment of the requirements for the degree

DOCTOR OF PHILOSOPHY

Department of Biology
College of Arts and Sciences

KANSAS STATE UNIVERSITY
Manhattan, Kansas

2026

Approved by:

Co-Major Professor
Laura Miller

Approved by:

Co-Major Professor
Susan Brown

# Copyright

# Abstract

Endogenous stem cells are responsible for tissue maintenance, remodeling, and repair in many organisms. This project explored whether signaling pathways associated with proliferation and apoptosis could be manipulated to alter endogenous stem cell activity during post-embryonic development, with long-term interest in how these mechanisms could eventually contribute to regenerative approaches. Initial pathway comparisons examined Wnt, Notch, TGF-β, and Hippo signaling. The Hippo pathway was selected for further investigation because of its direct involvement in regulation of proliferation, apoptosis, and tissue growth. *Tribolium castaneum* was chosen as the experimental model because its midgut contains accessible intestinal stem cell clusters (nidi) and supports strong systemic RNA interference (RNAi).

Double-stranded RNA targeting Hippo pathway components including *hippo*, *warts*, *yorkie*, and *salvador* were injected into larval, pupal, and adult stages. Midgut tissues were evaluated using EdU incorporation assays, fluorescence microscopy, histology, RT-qPCR, and RNASeq. Among the genes tested, *salvador* knockdown produced the strongest and most consistent phenotype. Midgut tissues displayed disrupted epithelial organization, widespread EdU incorporation, nuclear crowding, tissue fragility, and abnormal nidi morphology across developmental stages. Similar abnormalities were reproduced using an independent *salvador* dsRNA construct. RT-qPCR confirmed reduction of *salvador* transcript expression following RNAi treatment.

RNASeq analysis following *salvador* knockdown identified transcriptional changes associated with epithelial organization, ion transport, stress responses, and cytoskeletal regulation rather than a clear enrichment of canonical proliferative signatures. The observed

phenotype was therefore interpreted as dysregulated proliferative activity associated with loss of epithelial organization rather than controlled regenerative expansion.

This work supports the use of *Tribolium castaneum* as a model for studying Hippo pathway function during post-embryonic intestinal remodeling and demonstrates that disruption of *salvador* produces extensive abnormalities in proliferative regulation and midgut organization.

# Table of Contents

# List of Figures

# List of Tables

# List of Graphs

# Acknowledgements

Primarily, I'd like to acknowledge Dr. Brown, who has guided my professional development in this monumental career shift and helped me get acclimated to the world of bioinformatics and science. I'd also like to acknowledge Dr. Park for allowing me to use his facilities for insect rearing and experimentation, Dr. Miller for allowing me to use the equipment in her facilities and for taking on the role of Co-major professor when funding became an issue.

As there are too many people to individually list and to avoid running the risk of leaving anyone out, I'd like to extend a final thank you to everyone and anyone who participated in one way or another to the successful completion of this project.

# Dedication

For my family.

# Chapter 1 - Signaling pathways and endogenous stem cell proliferation in *Tribolium castaneum*

## Introduction

Over the last three decades, pluripotent stem cell research has become increasingly important in regenerative medicine because of its potential to restore damaged tissues and support genetic therapies [1,2]. This includes tissues with limited regenerative capacity, such as components of the nervous system [1]. Despite this potential, clinical application of stem cell therapies remains limited by several challenges. Exogenously cultured stem cells may be targeted by host immune responses following reintroduction, reducing treatment efficiency [1,2]. In addition, stem cell-based therapies are associated with substantial financial costs. Hematopoietic stem-cell transplantation (HSCT), for example, may cost hundreds of thousands of dollars per treatment attempt, with additional expenses associated with prolonged hospitalization and supportive care [3].

The Hippo signaling pathway regulates organ size, apoptosis, and cellular proliferation and has become an important target in cancer and regenerative biology research [4,5]. Genetic studies have shown that disruption of key Hippo effectors, including *YAP* (Yes-Associated Protein) */TAZ* (Transcriptional co-activator with PDZ-binding motif) in vertebrates and *yorkie* in invertebrates, alters proliferative activity in multiple tissue systems [6]. These observations raise the possibility that RNA interference (RNAi) mediated modulation of Hippo pathway components could influence endogenous stem cell proliferation outside of embryonic development. Because Hippo pathway activity is associated with regulation of both apoptosis and tissue growth, disruption of specific pathway components may alter the balance between proliferative activity and cell loss within regenerative tissues [5].

In *Drosophila melanogaster*, intestinal stem cells (ISCs) are distributed throughout the midgut epithelium (Fig. 1.1 a,b) and contribute to continuous tissue turnover and injury-induced regeneration [7,8]. This system has been extensively used to study ISC regulation under steady-state and stress conditions, including during remodeling associated with development and tissue repair.

**Figure 1.1 *Drosophila* Midgut Staining**

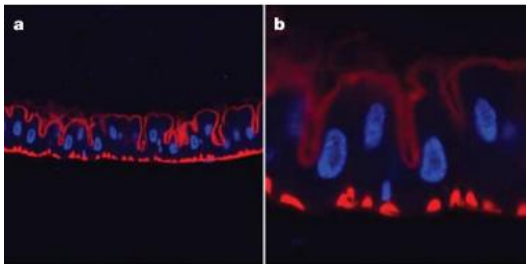


*Drosophila* midgut DAPI staining, revealing stem cell clusters (in blue) embedded in the epithelium of the intestines [7]. Red staining is done with phalloidin. The “hollow” appearance of phalloidin staining is characteristic of differentiated cells, allowing identification of distinct cell populations (stem cells and differentiated, non-stem cells). Reprinted from Nature, Volume 439, Micchelli, C. A. & Perrimon, N., Evidence that stem cells reside in the adult *Drosophila* midgut epithelium, Pages 475-479, Copyright (2005), with permission from Springer Nature.

**Figure 1.2 *Tribolium castaneum*'s Midgut**

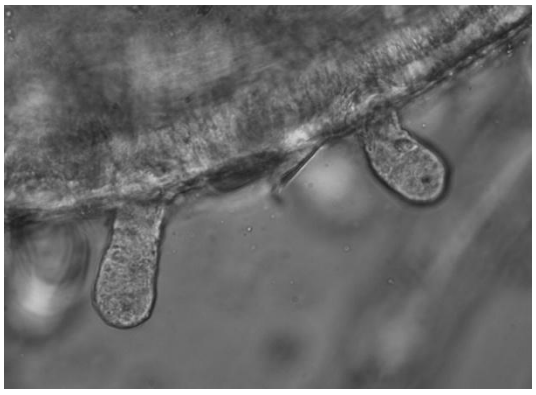

*Tribolium castaneum*'s midgut viewed at high magnification, evidencing the evaginated structures containing the stem cell clusters, called nidi. Source: author.

*Tribolium castaneum*, the red flour beetle, was selected as a model organism because its midgut contains distinct stem cell clusters (nidi, Figure 1.2) that are functionally comparable to mammalian intestinal stem cell compartments [9,10]. During metamorphosis, these clusters undergo temporally coordinated proliferation and differentiation, leading to large-scale remodeling of the midgut epithelium. This process occurs during hormonally regulated metamorphosis and provides access to a defined developmental window in which epithelial reorganization and stem cell dynamics can be examined [10].

These systems provide complementary contexts for studying stem cell–driven tissue dynamics.

## Stem cells in regenerative medicine and cancer pluripotency

### Therapeutic potential and challenges of hPSCs and MSCs

Human pluripotent stem cells (hPSCs) are defined by their ability to self-renew and differentiate into cell types derived from all three germ layers [1,2]. These properties have supported development of multiple *in vitro* differentiation approaches using feeder layers, conditioned media, and defined growth factor combinations [1,2]. Multipotent mesenchymal stem cells (MSCs) derived from bone marrow (BM), adipose tissue (AT), and umbilical cord (UC) have also been investigated for treatment of neurological, pulmonary, reproductive, and dermatological disorders [1]. Evidence suggests that MSC tissue origin may influence therapeutic potential. BM-MSCs have been associated with treatment of brain and spinal cord injuries, while AT-MSCs have been explored for reproductive disorders and skin regeneration, and UC-MSCs for pulmonary diseases [1]. Quantitative techniques including RT-qPCR, immunocytochemistry, and flow cytometry are commonly used to evaluate stem cell

differentiation and proliferative capacity [1,2]. These approaches are considered exogenous because stem cells are harvested from host tissues and later reintroduced following *in vitro* culture outside of the native extracellular environment [1,2].

Several limitations continue to restrict clinical application of these approaches. Stem cells expanded *in vitro* may trigger host immune responses following reintroduction, reducing treatment efficiency and regenerative potential [1,2]. In addition, procedures such as hematopoietic stem-cell transplantation (HSCT) are associated with substantial financial costs. Median healthcare expenses for HSCT may approach $290,000 within the first 100 days following transplantation, with additional costs associated with prolonged hospitalization and myeloablative treatment protocols [3].

Endogenous stem cells are tissue-specific stem cell populations that contribute to tissue maintenance and repair through controlled proliferation and differentiation [9,11]. Because these cells already reside within native tissue environments, stimulation of endogenous regenerative responses may avoid some limitations associated with exogenous stem cell transplantation [11]. However, the mechanisms regulating endogenous stem cell activation and tissue repair remain incompletely understood.

These limitations have increased interest in approaches that stimulate endogenous regenerative responses while reducing the risks and costs associated with exogenous stem cell transplantation. One potential strategy involves modulation of proliferative pathways through targeted RNA interference (RNAi) [36,37]. If endogenous stem cell populations can be stimulated in a controlled manner, this approach could provide an alternative framework for regenerative studies without the extensive culture and transplantation procedures required for exogenous stem cell therapies.

## Advances in skeletal regeneration and delivery systems

Both exogenous and endogenous approaches have been explored in skeletal regeneration [11]. Exogenous strategies typically involve expansion of stem cells *ex vivo* followed by transplantation using engineered scaffolds composed of synthetic polymers, such as polylactic acid (PLA) and polyglycolic acid (PGA), or natural matrices including collagen and gelatin [11,12]. These scaffolds are designed to support cell survival, tissue integration, and controlled differentiation within damaged tissues. Endogenous approaches instead focus on stimulating resident mesenchymal stem cell populations already present within host tissues to promote regenerative repair [11,13].

## Signaling pathways governing stem cell behavior

Stem cell behavior is regulated by several interconnected signaling pathways, including Wnt/β-catenin, Notch, TGF-β, and Hippo signaling. Previous studies in *Drosophila* have shown that Wnt/β-catenin signaling contributes to maintenance of intestinal stem cell proliferation and self-renewal [9,14]. Experimental manipulation of Wnt pathway activity has been associated with increased BrdU incorporation and elevated proliferative responses within the intestinal epithelium [9,14]. However, because Wnt signaling also plays major roles during early development, experimental disruption of this pathway can produce broad pleiotropic effects [9].

Targeted manipulation of Wnt signaling in adult tissues presents additional challenges because the pathway contributes to regulation of tissue homeostasis, proliferation, and differentiation. Alteration of this balance can produce abnormal proliferative responses and disrupt normal tissue organization. Increased Wnt activity has been associated with hyperplastic growth in multiple tissue systems, while disruption of Wnt pathway components in *Drosophila*

can produce broad developmental abnormalities rather than effects restricted to adult stem cell populations [9]. Although Wnt signaling is important for stem cell maintenance, its broad developmental and tissue-specific effects make targeted manipulation difficult in post-embryonic tissues.

Notch signaling contributes to regulation of stem cell differentiation and cell fate determination. Previous studies in mammalian intestinal organoids and *Drosophila* have shown that altered Notch activity affects differentiation of intestinal stem cell lineages [8,14]. Increased Notch signaling has been associated with differentiation toward absorptive enterocytes, whereas reduced pathway activity results in expansion of secretory cell populations [8,14]. In *Drosophila*, disruption of Notch signaling alters the balance between absorptive and secretory lineages within the intestinal epithelium. Notch pathway disruption also presents limitations for regenerative applications because altered signaling strongly affects epithelial differentiation patterns. Rather than selectively increasing stem cell proliferation, reduced Notch activity can shift lineage balance and produce disorganized intestinal architecture [8]. This makes controlled expansion of endogenous stem cell populations difficult without simultaneously disrupting normal epithelial organization.

TGF-β signaling is strongly associated with regulation of proliferation and differentiation in multiple stem cell systems. Experimental inhibition of TGF-β signaling can increase proliferative activity *in vitro*, whereas pathway activation promotes differentiation and expression of lineage-associated markers in mesenchymal stem cell cultures. Increased expression of collagen and smooth muscle actin, together with phosphorylation of SMAD proteins, has been used as evidence of TGF-β–mediated differentiation activity [15]. However, the effects of TGF-β disruption vary substantially across cell types and tissue environments. In

mesenchymal stem cell populations, inhibition of TGF-β signaling may increase cell division while impairing acquisition of normal differentiation markers, producing immature cell populations. In epithelial and progenitor tissues, similar disruption can alter tissue organization and interfere with normal cell fate regulation. Prolonged pathway inhibition may therefore increase proliferation at the expense of normal tissue architecture and cellular maturation.

Hippo signaling is a major regulator of stem cell proliferation, tissue growth, and apoptosis. Experimental studies in both *Drosophila melanogaster* and mammalian systems have shown that disruption of Hippo pathway activity alters proliferative behavior within stem cell populations [16,17]. In mouse intestinal tissue, increased *YAP* activity has been associated with elevated BrdU incorporation and expansion of stem cell compartments together with increased expression of stem cell-associated markers such as Lgr5 [16]. In *Drosophila*, RNAi-mediated disruption of Hippo pathway components results in nuclear localization of *yorkie* and increased expression of growth-associated targets including Cyclin E and diap1 [6,18].

The Hippo pathway regulates both proliferation and apoptosis through control of *YAP/TAZ* activity and has been strongly associated with tissue growth regulation in both vertebrate and invertebrate systems [5]. Increased nuclear localization of *YAP/TAZ* has also been associated with proliferative abnormalities and aggressive tumor phenotypes in several human cancers [5,19]. Compared with Wnt, Notch, and TGF-β signaling, Hippo pathway activity is more directly associated with regulation of tissue growth and proliferative control, making it a strong candidate for studies examining endogenous stem cell behavior during tissue remodeling and adult tissue maintenance [18,20]

**Comparative evaluation:**

Wnt/β-catenin signaling is required for stem cell maintenance and early developmental processes, but pathway activity in adult tissues is tightly regulated within stem cell niches [8,9]. Disruption of this balance can alter both proliferation and differentiation, producing expansion of undifferentiated cell populations and abnormal tissue organization rather than coordinated tissue growth. Notch signaling primarily influences lineage specification and differentiation within intestinal tissues and is less directly associated with stimulation of proliferative expansion [8]. TGF-β signaling is similarly linked to regulation of differentiation and cell cycle arrest, and pathway disruption may increase proliferation while simultaneously interfering with normal tissue organization and cellular maturation [15]. Because of its central role in tissue growth and proliferative regulation, Hippo signaling was selected for further investigation [16,17]. These characteristics made the Hippo pathway a strong candidate for investigating controlled modulation of endogenous stem cell behavior.

Manipulation of any major developmental signaling pathway can produce pleiotropic effects, whether through RNAi, CRISPR-mediated disruption, or other genetic approaches. The rationale for focusing on Hippo signaling was therefore not based on absence of pleiotropy, but rather on the pathway's more direct association with regulation of proliferation, apoptosis, and tissue growth through *YAP/TAZ* (*yorkie* in *Drosophila*) activity. Previous studies have shown that disruption of specific Hippo pathway components can strongly alter proliferative behavior within stem cell populations [16,17]. Compared with pathways that broadly regulate lineage specification or early developmental patterning, Hippo pathway modulation may provide a more direct framework for examining proliferative regulation within remodeling and adult tissues.

Experimental studies in *Drosophila* and murine systems have shown that disruption of Hippo pathway components directly alters cell cycle progression, proliferative activity, and cell

survival [5,6]. Although pleiotropic effects can occur following manipulation of any major signaling pathway, Wnt, Notch, and TGF-β signaling are more broadly associated with developmental patterning and lineage specification. Disruption of these pathways may therefore produce widespread effects on differentiation and tissue organization in addition to altered proliferation. Hippo signaling was selected for this study because of its more direct association with regulation of tissue growth, apoptosis, and proliferative control.

## Cancer stem cell pluripotency

Many tumors contain subpopulations of cancer stem cells (CSCs) that display extensive self-renewal and multilineage differentiation capacity similar to embryonic stem cells [21]. Studies examining metabolic regulation of CSCs have shown that maintenance of undifferentiated states depends on specific metabolic pathways. Inhibition of stearoyl-CoA desaturase 1 (SCD1), an enzyme involved in oleate synthesis, selectively induces death in undifferentiated CSC populations, whereas supplementation with exogenous oleate can partially restore cell survival [21]. These findings suggest that stem cell maintenance is closely associated with cellular metabolic state.

Similar relationships between stem cell maintenance, proliferation, and survival have been described in normal stem cell systems regulated by pathways including Hippo, Wnt, and Notch [4,22]. The overlap between regenerative and oncogenic signaling highlights the importance of controlled proliferative regulation when investigating mechanisms associated with tissue repair and stem cell activation.

# The Hippo pathway: discovery, conservation, mechanisms, and oncogenic implications

## Historical discovery through genetic screens

The Hippo pathway was initially characterized in *Drosophila melanogaster* through genetic mosaic screens in which loss-of-function mutations in genes such as *warts* (*Wts*) and *salvador* (*Sav*) produced extensive tissue overgrowth (in various tissues, such as eyes or wings) without major alteration of cell fate [6, 23] (Figure 3).

**Figure 1.3 Wild Type *D. Melanogaster* vs *hpo*/*wts* Mutant**

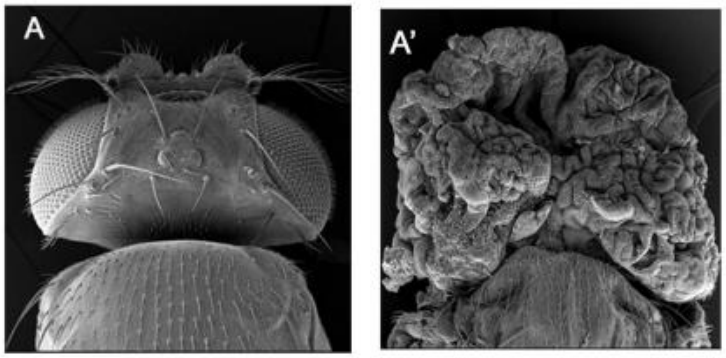


Wild type (A) D. Melanogaster vs *hpo/wts* mutant (A') showing uncontrolled tissue overgrowth [24]. Image was made available under the Creative Commins CC BY license and does not reflect the endorsement or recommendation of the authors.

Subsequent FLP/FRT-mediated mosaic analyses showed that mutations in *hippo* and *yorkie* produced similar overgrowth phenotypes, supporting the existence of a kinase cascade involved in regulation of organ size. These experiments demonstrated that coordinated signaling activity contributed to regulation of proliferation and apoptosis in developing tissues. The pathway also appears to be highly conserved across metazoans.

## Conservation of the Hippo pathway

The Hippo signaling pathway can be traced to early metazoans, with core pathway components displaying strong sequence and domain conservation [25]. These core elements (Fig. 1.4) are generally more conserved than many upstream or downstream regulators, reflecting their central role in regulation of epithelial proliferation, apoptosis, and organ size [25]. Functional conservation has also been supported by studies showing that *YAP*/*yorkie* orthologues retain growth-regulatory activity across multiple animal lineages [17]. Although sequence conservation is well established, functional validation in model organisms remains necessary to determine how pathway activity is maintained across species.

In *Tribolium castaneum*, larval RNAi targeting Hippo-associated genes such as Dachs and *yorkie* produces defects in elytron and hindwing development, supporting a role in post-embryonic tissue growth and patterning [26]. In *Drosophila*, disruption of Hippo pathway components including *warts* and *yorkie* results in tissue overgrowth and altered epithelial homeostasis [8,27]. Comparable phenotypes have also been observed in other insects. Disruption of Fat/Dachsous signaling affects appendage size in crickets [28], while *yorkie* activity in *Bombyx mori* contributes to regulation of organ growth during metamorphosis [29].

Disruption of Hippo pathway components produces similar growth-related phenotypes across insect systems, including increased proliferation, tissue overgrowth, and abnormal development, indicating that its role in restricting growth is conserved. Differences between species reflect variation in developmental context rather than a change in core pathway function.

**Figure 1.4 Hippo Signaling Pathway in Arthropoda and Mammalia**

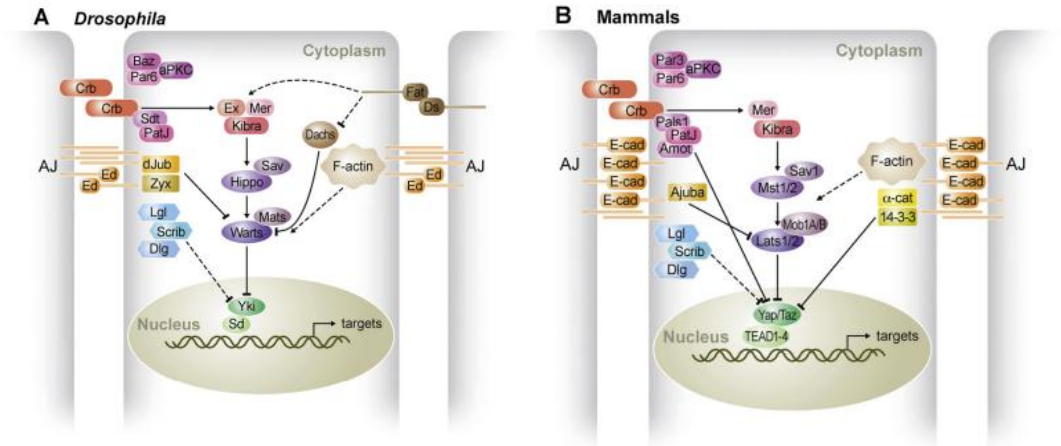


Hippo Signaling Pathway in Arthropoda and Mammalia shows remarkable conservation [30]. Reprinted from the Seminars in Cell & Developmental Biology, Volume 23, Issue 7, Schroeder, M.C. & Halder, G., Regulation of the Hippo pathway by cell architecture and mechanical signals, pages 803-811, Copyright (2012), with permission from Elsevier.

## Molecular mechanisms elucidated by experimental approaches

### Kinase cascade and phosphorylation dynamics

Genetic, biochemical, co-immunoprecipitation, and kinase studies demonstrated that *hippo* (*hpo*/*MST1/2*) phosphorylates and activates *warts* (*wts*/*LATS1/2*), which in turn phosphorylates *yorkie* (*yki*/*YAP/TAZ*) [4,16,20]. Phosphorylation of *yorkie* promotes its cytoplasmic retention through interaction with 14-3-3 proteins, preventing activation of pro-proliferative and anti-apoptotic target genes [4,6]. These studies identified the kinase cascade as a central mechanism through which Hippo signaling regulates tissue growth and proliferative activity.

### *salvador*/*SAV1/WW45*: Central adaptor in the cascade

*salvador* (*Sav*), also known as *SAV1* or *WW45* in mammals, functions as a central adaptor protein within the Hippo pathway. Genetic experiments in *Drosophila* demonstrated that loss of *salvador* promotes tissue overgrowth through disruption of cell cycle exit and apoptosis [23]. Reduced *salvador* activity interferes with activation of *warts*, leading to decreased phosphorylation of *yorkie* and increased nuclear accumulation [4,31]. *In vitro* kinase assays further demonstrated that *salvador* enhances *hippo*-mediated phosphorylation of *warts* [4]. Domain analyses have shown that the WW domains of *salvador* are required for pathway activity, and sequence comparisons indicate strong conservation across metazoans [25]. Clinical and molecular studies have also associated reduced *SAV1/WW45* expression with tumor progression, supporting its role as a tumor suppressor within the Hippo pathway [19,32].

### The role of Merlin and upstream regulation

*Merlin* (Mer, encoded by *NF2* in humans) functions as an upstream regulator of the Hippo pathway. Genetic and RNAi studies in *Drosophila* have shown that loss of Merlin produces tissue overgrowth phenotypes similar to those observed following disruption of core Hippo pathway components [5]. Merlin also interacts with proteins including Expanded (Ex) and Kibra to promote localization of Hippo pathway components at the plasma membrane [5,30]. Although the present study focuses primarily on *salvador*, *Merlin* provides additional context for upstream regulation of Hippo pathway activity

## Oncogenic implications and integration with other pathways

### *YAP/TAZ*/*yorkie* as proto-oncogenes

*yorkie* in *Drosophila* and its mammalian homologs *YAP* and *TAZ* are considered proto-oncogenic regulators because increased pathway activity promotes excessive cellular proliferation [5,20]. Transgenic overexpression studies in *Drosophila* and murine systems have

shown that elevated nuclear *YAP/TAZ* activity increases expression of genes associated with cell cycle progression and inhibition of apoptosis [4,16].

Clinical and immunohistochemical studies have further associated increased nuclear localization of *YAP/TAZ* with aggressive tumor phenotypes in colorectal, liver, and breast cancers [19]. Activation of upstream Hippo pathway components, including *salvador*, promotes phosphorylation and cytoplasmic retention of *YAP/TAZ*, restricting their proliferative activity [4,20].

Genetic disruption, RNAi-mediated knockdown, and transcriptomic analyses collectively support a central role for Hippo signaling in regulation of proliferation, apoptosis, and tumor suppression [4,16]

**Crosstalk with Wnt, Notch, and TGF-β signaling**

The Hippo pathway interacts with several signaling networks involved in stem cell maintenance and tissue homeostasis. Wnt/β-catenin signaling contributes to regulation of stem cell proliferation and differentiation, and Hippo pathway activity can influence Wnt-associated transcriptional responses [4,9,14]. Notch signaling regulates intestinal stem cell lineage specification, and interactions between Notch and Hippo signaling have been associated with maintenance of stem cell populations and epithelial differentiation [6,14,20]. TGF-β signaling similarly influences proliferation and differentiation in a context-dependent manner, and interactions between TGF-β and Hippo pathway components further contribute to regulation of tissue organization and cellular behavior [4,20]. These interactions suggest that Hippo signaling functions within a broader regulatory network involved in stem cell activity and tissue homeostasis.

# *Tribolium castaneum* as a model for endogenous intestinal stem cell proliferation

## *Tribolium castaneum* developmental stages

*Tribolium castaneum* undergoes complete metamorphosis through four major developmental stages: embryo (egg), larva, pupa, and adult [33,34]. The larval stage consists of multiple growth phases, or instars, separated by molting events as the organism increases in size [34]. The final larval stage, commonly referred to as the last instar or "C-shaped" stage because of the characteristic body posture of the larvae, immediately precedes pupation and marks the onset of developmental remodeling. During the pupal stage, extensive tissue reorganization takes place, including degeneration of larval tissues and formation of adult structures [10,35].

## Structural and developmental features of the *Tribolium* midgut

The midgut of *Tribolium castaneum* provides a useful system for studying post-embryonic intestinal remodeling and stem cell proliferation. Unlike *Drosophila melanogaster*, where intestinal stem cells are distributed throughout the midgut epithelium, the *Tribolium* midgut contains distinct stem cell clusters referred to as nidi (Figure 1) that resemble mammalian intestinal crypt structures [9,22]. *Tribolium* has also been widely used as a developmental and genetic model organism for several decades. Parthasarathy and Palli (2008) characterized midgut remodeling during metamorphosis and showed that larval polyploid cells (LPCs) undergo programmed cell death while intestinal stem cells proliferate to reconstruct the adult midgut epithelium [10]. Their work further demonstrated that ISC proliferation increases between 24 and 48 hours following pupation, corresponding to the period during which nidi formation and adult gut reorganization occur.

### Parthasarathy and Palli (2008) findings [10]

Parthasarathy and Palli (2008) provided detailed characterization of intestinal stem cell dynamics during *Tribolium* metamorphosis [10]. Figure 1.5 illustrates the developmental progression into adulthood, including periods of increased proliferative activity during metamorphosis.

**Figure 1.5 Tissue Remodeling in Larval Midgut and Nidi Evagination**

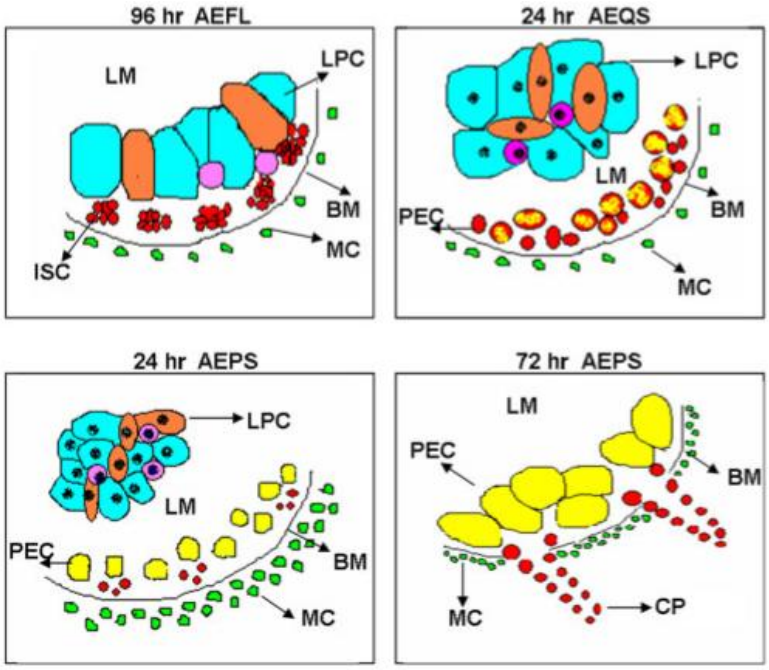


Early C-Shaped larvae (AEFL) undergoing apoptosis of Larval polyploid cells (LPC) and moving into the lumen (LM), as well as the intestinal stem cells (ISC) pushing through the basement membrane (BM), forming the epithelium and evaginating into nidi (crypts, CP) [10]. Reprinted from Developmental Dynamics, Volume 237, Issue 4, Parthasarathy, R. & Palli, S.R., Proliferation and differentiation of intestinal stem cells during metamorphosis of the red flour beetle, *Tribolium castaneum*, pages 893-908, Copyright (2008), with permission from John Wiley and Sons.

During larval development, the midgut is primarily composed of larval polyploid cells (LPCs), which carry out digestive functions. As the organism prepares for metamorphosis, these cells are destined for elimination, coinciding with the transition to the characteristic “C-shaped” configuration marked by reduced movement and body contraction [10].

Following ecdysis into the pupal stage, LPCs undergo programmed cell death, as demonstrated by TUNEL assays. At the same time, a population of intestinal stem cells begins to proliferate, as shown by BrdU incorporation and phospho-histone H3 staining. Proliferation peaks between 24 and 48 hours after pupal ecdysis (AEPS), corresponding to the period during which the adult midgut epithelium is reconstructed [10].

This proliferation and subsequent differentiation lead to the formation of organized stem cell clusters (nidi), which function as the adult stem cell niche. RNAi targeting the ecdysone receptor disrupts this process, resulting in delayed LPC clearance and impaired nidi formation. These findings demonstrate, through morphometric and molecular analyses, that hormonal signaling is required for proper ISC-mediated midgut remodeling [10].

Using precise RNAi injections, dosage testing, hormonal treatments, and rigorous quantification, Parthasarathy and Palli (2008) established a detailed timeline and mechanism for midgut regeneration in *Tribolium* [10]. Their work has been instrumental in advancing our understanding of how larval stem cell populations transition into organized adult niches during metamorphosis, which in turn informs strategies to harness endogenous regenerative processes.

## Detailed experimental approaches in *Tribolium*

### dsRNA synthesis, injection, and dosage testing

RNAi efficacy in *Tribolium castaneum* has been evaluated using both dsRNA feeding and injection approaches [36,37]. Injection-based delivery generally produces more consistent knockdown because it bypasses degradation associated with oral uptake and allows direct entry of dsRNA into the hemocoel [37]. The systemic nature of RNAi in *Tribolium* allows dsRNA to spread throughout the organism, resulting in systemic gene silencing [39]. Sustained reduction of

target transcript levels across multiple time points has been confirmed using RT-qPCR analyses [36,38].

Templates for dsRNA synthesis are generated by PCR amplification using gene-specific primers containing T7 promoter sequences. *In vitro* transcription with T7 RNA polymerase is followed by purification procedures such as phenol-chloroform extraction and isopropanol precipitation to obtain high-quality dsRNA [36].

Injection procedures vary according to developmental stage. For larval RNAi, last-instar larvae are immobilized on a cold block prior to microinjection into the dorsal abdomen [38]. Dose-response relationships can then be evaluated through RT-qPCR analysis of transcript reduction following dsRNA administration [36,39]. For pupal RNAi, injections are commonly performed within the first 0–6 hours after ecdysis (AEPS, Figure 5), corresponding to the period of extensive midgut remodeling [10]. In adults, insects are typically anesthetized with ether prior to dsRNA delivery into the hemocoel through the ventral abdomen or beneath the elytra, allowing systemic knockdown throughout the organism. This approach has been widely used in large-scale functional RNAi screens examining phenotypes such as lethality, fertility defects, and morphological abnormalities following gene silencing [39].

**Quantification and validation of RNAi effects**

Total RNA extracted from dissected midgut tissues is reverse-transcribed, and gene expression is quantified using RT-qPCR. Expression levels are normalized to housekeeping genes such as RpL32 and reported as ΔΔCt values to evaluate knockdown efficiency [10,36].

Cell proliferation is assessed using immunohistochemistry and nucleotide incorporation assays. Immunostaining for phospho-histone H3 identifies mitotic intestinal stem cells, while BrdU incorporation labels cells undergoing DNA synthesis, allowing spatial and temporal

evaluation of proliferative activity. These approaches have been used to show that disruption of hormonal signaling pathways, including the ecdysone receptor, reduces ISC proliferation and delays programmed cell death in larval progenitor cells [10]. EdU (5-ethynyl-2′-deoxyuridine) incorporation assays similarly measure S-phase entry through a Click-iT reaction, binding fluorescently tagged molecules to newly synthesized DNA, that enables fluorescent visualization of proliferating cells using confocal microscopy. This method has also been applied in *Drosophila* to assess intestinal stem cell proliferation and epithelial remodeling [8,14].

Apoptosis is evaluated using TUNEL assays, which detect DNA fragmentation within midgut tissues. These analyses are primarily used to assess the presence and distribution of apoptotic fragments within larval progenitor cell populations rather than to generate quantitative measurements. Histological sections stained with hematoxylin and eosin provide structural context for TUNEL-positive cells and allow comparison between control and RNAi-treated tissues [10].

RNA sequencing (RNA-seq) is used to assess transcriptome-wide changes in gene expression following RNAi-mediated knockdown. In stem cell systems including the *Drosophila* midgut, RNA-seq has been applied to characterize transcriptional responses associated with altered proliferation and differentiation [14,22]. In the context of Hippo signaling, pathway perturbation has been associated with changes in downstream *YAP*/*yorkie* target gene expression [4]. This approach enables broader evaluation of transcriptional responses following pathway disruption.

**Hormonal regulation experiments**

The roles of 20-hydroxyecdysone (20E) and juvenile hormone (JH) in midgut remodeling have been examined using *in vitro* culture of dissected tissues. Incubation of midguts in

Schneider's medium supplemented with 20E (1 μM) increases intestinal stem cell (ISC) proliferation, accompanied by elevated BrdU incorporation and increased expression of mitotic markers. Treatment with JH (100 nM), however, is associated with reduced ISC proliferation, suggesting opposing effects of 20E and JH during midgut remodeling [10].

RNAi targeting ecdysone receptor isoforms, particularly EcRA and its cofactor USP, impairs ISC proliferation and delays clearance of larval progenitor cells (LPCs). These effects are associated with altered mitotic index and abnormal epithelial morphology relative to control tissues, supporting a central role for ecdysone signaling during metamorphic gut remodeling [10].

**Orthologue analysis and comparative insights**

The Hippo signaling pathway can be traced to early metazoans, with core pathway components displaying stronger sequence conservation than many upstream or downstream regulators [25]. This conservation reflects the central role of the pathway in regulation of tissue growth and organ size through modulation of *yorkie*/*YAP* activity [16,17]. Comparative genomic analyses have identified orthologues of major Hippo pathway genes across insects, including *Drosophila melanogaster* and *Tribolium castaneum* [25,33]. Genome analysis of *T. castaneum* identified homologs of multiple Hippo pathway components, indicating that the pathway is conserved at the sequence level within this species [33].

In *Drosophila*, Hippo pathway activity regulates intestinal stem cell (ISC) proliferation and epithelial homeostasis, and disruption of components such as *warts* and *yorkie* increases ISC proliferation and alters epithelial organization [8,27]. Functional involvement of *Hippo*-associated genes in *Tribolium* has also been demonstrated through larval RNAi targeting of *Dachs* and *yorkie*, which disrupts elytron and hindwing development during post-embryonic

growth [26]. Comparable studies in *Drosophila* have shown that disruption of Hippo pathway activity increases mitotic activity and promotes accumulation of undifferentiated progenitor cells within the midgut epithelium [27,40].

## Discussion

Research on stem cell regulation, Hippo signaling, and the use of *Tribolium castaneum* as an experimental system provides a framework for examining how transient modulation of this pathway influences tissue-level responses. Limitations associated with exogenous stem cell transplantation, including cost and immune compatibility [3], have increased interest in approaches that promote regenerative activity within endogenous tissues. The Hippo pathway is particularly relevant because it directly regulates proliferation and apoptosis through components such as *salvador*/*WW45* and *Merlin* [4,23]. However, increased *YAP/TAZ* (*yorkie*) activity is also associated with tumorigenic outcomes, indicating that pathway disruption must be carefully regulated [19,20].

*Tribolium castaneum* provides a useful system for studying post-embryonic intestinal remodeling and stem cell proliferation. Experiments using larval and pupal dsRNA injections, together with the systemic nature of RNAi in *Tribolium*, demonstrate that temporal regulation of gene expression is required for proper midgut remodeling and nidi formation [10,36,38]. Parthasarathy and Palli (2008) further showed that hormonal signaling through 20-hydroxyecdysone (20E) and juvenile hormone (JH) regulates intestinal stem cell proliferation during the transition from larval to adult midgut organization [10].

Interactions between Hippo signaling and pathways including Wnt, Notch, and TGF-β further indicate that proliferative regulation occurs within a broader signaling network. Understanding how these pathways interact may help clarify how proliferative responses can be

modulated without inducing uncontrolled tissue growth. Because *salvador*/WW45 promotes phosphorylation-dependent inhibition of *YAP/TAZ* activity, modulation of *salvador*-associated pathway activity may represent one mechanism through which proliferative responses could be regulated while limiting excessive *YAP/TAZ*-driven transcriptional activity [4,20,41]. Although the systemic RNAi response in *Tribolium* provides a powerful model for studying gene function during post-embryonic development, direct translation to vertebrate systems remains limited because long double-stranded RNA can activate innate immune responses, including interferon signaling [42]. Vertebrate RNAi approaches therefore more commonly rely on short interfering RNAs (siRNAs) delivered through targeted systems such as lipid nanoparticles [39].

## Conclusion

The studies reviewed above establish three major areas relevant to the present work: regulation of stem cell behavior in vertebrate and *Drosophila* systems, the role of Hippo signaling in controlling proliferation and apoptosis, and the established use of RNA interference in *Tribolium castaneum*. Experimental approaches including dsRNA synthesis, larval and pupal RNAi injections, systemic RNAi, dosage testing, and hormonal manipulation provide a framework for examining midgut remodeling and nidi formation during metamorphosis. The molecular characterization of Hippo pathway components in *Drosophila*, including *salvador*/*SAV1*/*WW45* and Merlin, further provides mechanistic context for regulation of tissue growth, proliferation, and apoptosis. At the same time, the oncogenic activity associated with deregulated *YAP/TAZ* (*yorkie*) highlights the importance of controlled pathway modulation.

Features of the *Tribolium* system, including accessible midgut stem cell clusters (nidi) and strong systemic RNAi responses, allow examination of stem cell proliferation during post-embryonic development and metamorphic remodeling. Interactions between Hippo signaling and

pathways such as Wnt, Notch, and TGF-β are also likely important for coordinating proliferation and differentiation during these processes.

The literature outlined above provides the basis for the experimental approach used in this study. RNA interference–mediated knockdown of Hippo pathway components was performed during larval, pupal, and adult stages, with particular focus placed on *salvador* because of its role in regulating downstream effectors such as *yorkie* and its association with apoptosis. RNAi was selected rather than genome-editing approaches such as CRISPR/Cas9 because it allows transient modulation of pathway activity without permanent disruption of essential regulatory genes. These experiments were designed to examine whether temporary disruption of Hippo pathway activity alters proliferative behavior during post-embryonic tissue remodeling and adult tissue maintenance.

# Chapter 2 - RNAi analysis of Hippo pathway genes in pupal, larval, and adult stages of *Tribolium castaneum*

## Introduction

Regulation of tissue growth and cellular proliferation is required for proper development and tissue maintenance. These processes are coordinated by signaling pathways that control cell division, differentiation, and programmed cell death to maintain tissue organization and structural integrity [1,2]. Stem cell proliferation is particularly important in epithelial tissues, where disruption of proliferative control can alter tissue architecture and homeostasis [8,9]. Controlled manipulation of these pathways has therefore become an area of interest in regenerative biology because of its potential to promote tissue repair through endogenous stem cell populations [1,11].

The Hippo signaling pathway is a major regulator of tissue growth and organ size, with evolutionary origins tracing back to metazoans [4]. Within the canonical pathway, *hippo* and *warts* act as upstream inhibitory regulators that restrict *yorkie* activity, while *salvador* functions as a scaffold protein facilitating kinase complex assembly [6,23]. Disruption of Hippo pathway activity has been associated with excessive tissue growth and loss of normal growth restriction in multiple model systems [6,23].

Studies in *Drosophila melanogaster* have shown that disruption of Hippo signaling produces tissue overgrowth phenotypes, including enlargement of the compound eye [6]. Work in the *Drosophila* midgut further demonstrated that Hippo signaling regulates intestinal stem cell homeostasis through inhibition of the transcriptional coactivator *yorkie* [43,44]. Loss of pathway activity increases stem cell division and produces epithelial hyperplasia within the intestinal epithelium [43,44].

These findings support a role for Hippo pathway activity in maintenance of proliferative balance during development. In *Drosophila melanogaster*, intestinal stem cells are embedded within the midgut epithelium, making direct visualization of proliferative compartments more difficult [8,14]. The midgut of *Tribolium castaneum* contains morphologically distinct stem cell clusters known as nidi [10]. These clusters contribute to intestinal epithelial renewal and provide a tissue environment in which disruption of proliferative organization can be more readily observed following genetic interference. Their compartmentalized organization is also analogous to mammalian intestinal crypts, where Hippo pathway activity has similarly been implicated in regulation of intestinal stem cell behavior [45].

RNA interference has become a standard tool for investigating gene function in *Tribolium castaneum* because of this beetle's robust systemic RNAi response, allowing efficient knockdown of target genes after a single dsRNA injection [36]. By delivering double stranded RNA directly into the hemocoel, gene expression can be suppressed without the need for transgenic insect lines. This approach has been successfully applied across larval, pupal, and adult stages [36,38,46]. Because RNAi produces transient suppression rather than permanent genomic modification, phenotypic effects may also be examined without stable genetic alteration.

During metamorphosis, pupae undergo extensive tissue remodeling that includes histolysis, cellular proliferation, and reorganization of adult structures, whereas larvae retain proliferative tissues that later contribute to adult tissue formation during metamorphosis [10]. Adults possess a comparatively stable anatomy. These physiological differences can influence dsRNA uptake, distribution, and phenotype manifestation following knockdown, meaning observations made in one developmental stage may not fully reflect responses in another.

Initial experiments in this study were performed during the pupal stage because metamorphosis involves extensive tissue remodeling, cellular turnover, and proliferative activity associated with formation of adult structures [10]. These processes created conditions in which disruption of Hippo pathway activity could produce detectable phenotypes. Pupae also provided practical advantages for experimental manipulation because they are immobile and can be collected at defined developmental intervals. Larvae require cooling prior to injection because of continuous movement, while adults must be anesthetized before handling.

Previous RNAi studies in *Tribolium castaneum* have frequently used pupal injections to evaluate developmental phenotypes [26,36]. Initial screening at this stage allowed rapid assessment of survival, lethality, and visible morphological abnormalities before proceeding to more time-intensive experiments in larvae and adults. These experiments identified stage-specific phenotypes associated with disruption of Hippo pathway components, particularly the distinct midgut phenotype observed after *salvador* knockdown.

## Methods

All experiments were performed with five biological replicates to ensure statistical significance. The *Tribolium castaneum* GA1 (Georgia 1) strain was used for every assay.

**Insect rearing** – Colonies were maintained under standard conditions that included variable humidity, a temperature of 32.5 °C, and variable light cycles. Colonies were cultured on organic, pesticide-free flour supplemented with 5% yeast.

- **Pupae** – Experimental pupae were obtained from a subculture that had been generated by transferring approximately 50 adults into a fresh colony. Pupae were collected roughly two weeks after the subculture was established 2.

- **Larvae** – Larvae were harvested from one of the subcultured colonies and staged to the L6 developmental stage. Staging was initially performed by measuring total larval length and later by measuring head capsule width (0.5–0.7 mm) under an optical microscope. To prevent damage during injection, a metal block that had been kept at –20 °C was placed beneath the injection plate.
- **Adults** – Adults were collected as larvae from a subcultured colony, allowed to complete eclosion, and injected under the elytra 1–2 days after eclosion. Prior to injection, adults were anesthetized by placing them on a mesh receptacle inside a dimethyl ether bottle for 2 minutes 30 seconds.

## Identification of gene targets and dsRNA design

Hippo pathway gene orthologs were identified in *Tribolium castaneum* using BLAST searches with *Drosophila melanogaster* reference genes obtained from NCBI [47]. Candidate orthologs were further evaluated by reciprocal BLAST analysis. Conserved coding regions were selected for primer design. Targeted regions were used to generate amplicons ranging from 250 base pairs to 600 base pairs, with most targets exceeding 400 base pairs in length, consistent with previously reported parameters influencing RNAi efficiency in *Tribolium* [38].

Primers were ordered from Integrated DNA Technologies with the T7 promoter sequence TAATACGACTCACTATAG appended to the 5’ end of both forward and reverse primers to enable bidirectional *in vitro* transcription.

PCR amplification was performed for each selected Hippo pathway target using cDNA generated from day 4 pupae as template. Gene-specific primers containing T7 promoter sequences appended were used to generate transcription-ready PCR products for dsRNA synthesis. Standard thermocycler conditions were used for amplification, consisting of an initial

denaturation step followed by 35 cycles of denaturation, primer annealing, and extension, and a final extension step. Annealing temperatures were adjusted according to the predicted melting temperature of each primer pair, and extension times were modified based on expected amplicon length.

## Validation of PCR products and dsRNA templates

All PCR amplified DNA products generated for dsRNA synthesis were validated by agarose gel electrophoresis prior to *in vitro* transcription. PCR products were resolved on a 1% agarose gel/TRIS acetate buffer and visualized to confirm the presence of a single amplicon of the expected size for each gene target. Only reactions producing a single discrete band were used for downstream dsRNA synthesis. This validation step was performed to ensure template specificity and to minimize the likelihood of off target dsRNA production.

## dsRNA synthesis and preparation

dsRNA was synthesized using the HiScribe T7 High Yield RNA Synthesis Kit E2040S according to the manufacturer's protocol [38]. Following transcription, dsRNA was purified as specified by the kit workflow. dsRNA concentration and purity were evaluated using Nanodrop spectrophotometry. All dsRNA preparations were aliquoted to avoid repeated freeze-thaw cycles and were diluted to a final concentration of 1 ng/nL prior to injection. Injection volumes of 100 nL therefore delivered approximately 100 ng of dsRNA per individual.

## Capillary needle pulling

A horizontal capillary needle puller (SUTTER INSTRUMENT CO. Model P-87) was employed to create the injection needles. The capillary was secured in horizontal clamps, heated until softened, and pulled apart to produce two precise, symmetrical needles with tip diameters as small as 0.02 μm.

## Injection procedure

Capillary needles were first filled with heavy mineral oil to displace any air and to prevent bubble formation. Subsequently, the needles were attached to a microinjector (nanojet), which was used to guarantee a controlled injection volume of 100 nanoliters. The needles were beveled (the tip was broken at an angle) to improve flow rates. Injection material (dsRNA, EdU, or distilled water) was pipetted onto a sterile plate and was drawn into the capillary needle and injected into the insect using the "WITHDRAW" and "INJECT functions of the microinjector.

## Post injection time points and sample collection

For pupal injections, individuals were monitored through the pupation period and were collected either upon full eclosion to adulthood or at the time of mortality if death occurred during the pupal stage.

For larval injections, early L6 larvae were collected at 24 hours and 48 hours post injection. Larvae were dissected at the designated time points to assess tissue level responses.

For adult injections, one-to-two-day old adults were collected at 12 hours and 24 hours post injection. After gross abnormalities were assessed visually, midgut dissections were performed at each time point to capture early and later responses following injection.

## EdU labeling, detection, and nuclear counterstaining

5-ethynyl-2′-deoxyuridine (EdU) incorporation was used to assess proliferative activity through labeling of newly synthesized DNA during S-phase. EdU labeling was performed using the Invitrogen Click iT EdU Cell Proliferation Kit for Imaging with Alexa Fluor 488 dye according to the manufacturer's (Thermo Fisher, Catalog number C10337) instructions. All reagents were prepared as instructed by the protocol and were protected from light where applicable.

## EdU preparation and injection

EdU working solutions were prepared according to the manufacturer's protocol and were diluted into the injection compatible buffer used for insect injections. When co- injected with dsRNA, dsRNA solutions were first normalized to the desired concentration, after which EdU was added to achieve the final working concentration without altering dsRNA dosage. The final injection solution was mixed gently until homogeneous and was loaded into capillary needles for injection. Injection volume and delivery parameters matched those used for dsRNA injections. Because no established EdU injection protocol was available for *Tribolium castaneum*, the procedure was adapted from existing Thermo Fisher Click-iT EdU protocols designed for tissue soaking in small organisms and in vivo mouse injections. Modifications included delivery of EdU by direct hemocoel microinjection rather than tissue soaking or mammalian injection, use of injection volumes appropriate for insect body size, and co-injection of EdU with dsRNA when proliferation was assessed after RNAi treatment.

## Pupal stage injection of *Hippo* pathway dsRNA

Pupal injections were performed using 100 nanogram/nanoliter normalized dsRNA targeting *hippo*, *warts*, *yorkie*, and *salvador*. For each gene, 20 pupae were injected per replicate, and each experiment was performed across five biological replicates. For control in each experiment, 20 additional individuals were injected with nuclease-free (NF) water (highly purified, DEPC-free water certified to be free of both DNase and RNase enzymes) (100 nanoliters). Injected individuals were monitored for survival, timing of lethality, successful eclosion, and adult gross morphology. Representative images were collected for each condition.

## Larval staging

Initial larval staging was performed by measuring overall body length. During an 8-week observational period, substantial variability between measured body length and apparent larval stage was noted. Body length measurements fluctuated depending on larval posture and degree of contraction at the time of measurement, which complicated consistent staging using this metric.

Following this observational period, larval staging was performed using head capsule width measurements. Head capsule width was measured using the graded scale present in the optical microscope eyepiece. Measurements obtained using this approach were consistent across repeated observations (between 0.65 and 0.74 mm) and were less influenced by larval positioning. Head capsule width was therefore used as the staging metric for all subsequent larval injection experiments. Representative measurements are shown in Table 2.1 [48]. Park, however, noted these measurements are also variable based on insect strain and rearing conditions, but reliable within the same setting [48].

**Table 2.1 *Tribolium castaneum* Head Capsule Width Measurements Across Different Larval Instars**

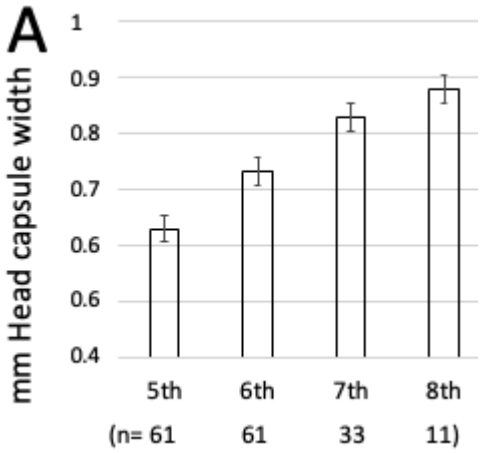


*Tribolium castaneum* head capsule width measurements across different larval instars. 7th and 8th instar are related to Goliath mutant strain and not included in our study [48]. (Yoonseong Park, Park Lab, Department of Entomology, Kansas State University, 2023).

## Larval injection and time point analysis

Early L6 larvae were injected and dissected at 24 and 48 hours post injection prior to pupation. Each experimental condition was performed with n = 20 larvae per replicate across five biological replicates.

EdU was co-injected with dsRNA in all experimental groups. A total injection volume of 200 nanoliters was delivered per larva, consisting of 100 nanoliters of dsRNA solution and 100 nanoliters of EdU solution. Control larvae received 100 nanoliters of NF water co injected with 100 nanoliters of EdU, for a total injection volume of 200 nanoliters.

A rate of injection failure comparable to that observed in pupal experiments was recorded. Individuals that died within 24 hours post injection were classified as injection failures and were excluded from downstream tissue analysis.

Proliferative activity within the midgut was assessed qualitatively using EdU incorporation at both 24 and 48 hours post injection. Apoptotic activity was assessed using a

TUNEL end point assay at 48 hours post injection. The 48 hour time point was selected for TUNEL analysis based on prior reports indicating that apoptotic activity peaks during late larval development preceding pupation [10]. Nuclear morphology was visualized using DAPI staining.

Dissections of *salvador* dsRNA injected larvae were technically challenging due to reduced tissue integrity. In wild type control larvae, successful midgut dissection was achieved in approximately 95% of individuals. However, successful dissection of *salvador* dsRNA injected larvae was achieved in approximately 30 to 40% of individuals. Out of 20 injected larvae per replicate, between 6 and 8 individuals yielded intact midgut tissue with enough integrity left for imaging.

## Adult injections and time point analysis

To validate observations obtained in earlier life stages, dsRNA targeting *hippo*, *warts*, *yorkie*, and *salvador* were also injected into adult individuals. Adults were analyzed at 24 hours post injection for all gene targets.

Due to the pronounced phenotype previously observed following *salvador* knockdown in other life stages, *salvador* injected adults were additionally analyzed at 12 hours post injection to evaluate the onset of the observed phenotype.

EdU was co injected at the same volume used in larval experiments. A total injection volume of 200 nanoliters was delivered per individual, consisting of 100 nanoliters of dsRNA solution and 100 nanoliters of EdU solution. Control adults received 100 nanoliters of nuclease-free (NF) water co injected with 100 nanoliters of EdU, for a total injection volume of 200 nanoliters.

## Tissue dissection conditions

All tissues were dissected in phosphate buffered saline (PBS) to maintain isotonic conditions and preserve tissue integrity during handling. Tissues were maintained submerged in buffer throughout dissection and transfer steps until fixation or downstream processing.

## Fixation and permeabilization

Following dissection, tissues were fixed immediately in a 4% formalin solution for 30 minutes to preserve incorporated EdU signal. Fixed tissues were washed using 3% bovine serum albumin to remove residual fixative and reduce nonspecific binding. Tissues were permeabilized using 0.05%Triton X-100 to permit access of click chemistry reagents to incorporate EdU. Additional washes were performed using 3% bovine serum albumin following permeabilization.

## Click chemistry detection of EdU

EdU incorporation was detected using copper catalyzed click chemistry with Alexa Fluor 488 according to the manufacturer's protocol. A fresh reaction cocktail was prepared immediately prior to use and was applied to permeabilized tissues at the recommended reaction volume. Samples were incubated protected from light for the duration specified by the protocol. Following incubation, tissues were washed repeatedly using 3% bovine serum albumin to remove unbound fluorophore and to reduce background signal.

## TUNEL end point assay

Apoptotic DNA fragmentation was detected using a fluorescent TUNEL end point assay performed on non- embedded tissues. The TUNEL Assay Apoptosis Detection Kit with CF®594 conjugated nucleotides (catalog number 30064) obtained from Biotium was used according to the manufacturer's instructions.

Tissues were processed for the TUNEL assay following fixation and permeabilization. All reagents were prepared immediately prior to use as instructed by the manufacturer's protocol.

Samples were equilibrated in the buffer provided with the kit prior to initiation of the labeling reaction. The TUNEL reaction mixture was prepared immediately before application and was applied to tissues at the recommended reaction volume. Incubation was performed under the conditions specified by the manufacturer to allow incorporation of CF®594 labeled nucleotides at sites of DNA strand breaks.

Following completion of the labeling reaction, tissues were washed with 3% BSA thoroughly to remove unincorporated reagents and to reduce background fluorescence. Labeled tissues were maintained protected from light.

The TUNEL assay was performed as the terminal enzymatic labeling step prior to nuclear counterstaining.

## DAPI nuclear staining

Following completion of the EdU click reaction and wash steps, tissues were incubated in DAPI staining solution for five minutes to label nuclear DNA. Staining was performed protected from light. After incubation, tissues were washed using 3% BSA to remove excess DAPI prior to mounting.

## Mounting and imaging

Stained tissues were mounted using an antifade mounting medium and were stored protected from light until imaging. Imaging was performed using fluorescence microscopy with appropriate excitation and emission settings for Alexa Fluor 488 and DAPI (and TUNEL if applicable). Acquisition parameters were held constant within experiments to permit comparison across samples.

## Formalin fixed paraffin embedded tissue processing

### Fixation

Immediately following dissection, tissues were fixed to preserve morphology and structural integrity. Fixation was performed using 4% paraformaldehyde. Tissues were fixed for approximately three hours at room temperature or overnight at 4 degrees Celsius.

### Washing

Following fixation, tissues were washed three times in PBST consisting of phosphate buffered saline containing 0.05% Triton X-100. Each wash was performed for 20 minutes with gentle agitation.

### Dehydration

Tissues were dehydrated through a graded ethanol series to remove water content. Sequential incubations were performed in 50%, 70%, 80%, 90%, and 100% ethanol. Each step was performed for 10 to 15 minutes.

### Clearing

Following dehydration, tissues were transferred to 100% chloroform and incubated for a minimum of one hour and up to overnight to achieve clearing. For tissues exhibiting extensive sclerotization, a brief treatment was performed by adding one drop of propylene oxide for approximately 10 seconds, followed by immediate removal.

### Paraffin infiltration

Cleared tissues were infiltrated with molten paraffin wax maintained at 56 to 57 degrees Celsius. Paraffin infiltration was performed at 57 to 58 degrees Celsius for 12 hours or overnight. Tissues were maintained in the same paraffin solution or the paraffin was replaced up to two times prior to overnight incubation to improve infiltration efficiency.

**Embedding and block preparation**

Following infiltration, tissues were oriented in embedding molds and embedded in fresh paraffin. Embedded blocks were cooled at 4 degrees Celsius for a minimum of one hour prior to sectioning. Paraffin blocks were stored at 4 degrees Celsius and remained suitable for long term storage for extended periods.

**Sectioning**

Paraffin embedded tissues were sectioned using a microtome. Sections were cut at a thickness ranging from 6 to 10 micrometers. Sectioning was performed at a blade angle of approximately 5 to 6 degrees to facilitate ribbon formation.

**Slide mounting and drying**

Section ribbons were transferred onto charged glass slides coated with 0.5% gelatin solution. Slides were placed on a hot plate maintained at 35 to 37 degrees Celsius to promote section adhesion. Slides were allowed to dry overnight.

**Deparaffinization**

Prior to downstream applications, slides were deparaffinized by immersion in xylene solution. Deparaffinization was performed using two sequential incubations of 10 to 15 minutes each.

**Rehydration**

Deparaffinized slides were rehydrated through a graded ethanol series with decreasing ethanol concentrations. Slides were sequentially incubated from 100% ethanol to 50% ethanol, with each step performed for 10 to 15 minutes. Following rehydration, slides were transferred to aqueous buffer.

**Storage prior to staining**

Following rehydration, slides were stored in PBST containing 0.05% sodium azide to prevent microbial contamination. Slides were maintained under these conditions until use for immunohistochemistry or other downstream applications.

**Fluorescence visualization and microscopy**

Preliminary assessment of tissue morphology and staining quality was performed using an optical microscope. This approach was used to verify tissue integrity, gross morphology, and nuclear labeling (using DAPI staining) prior to advanced fluorescence imaging.

High resolution fluorescence imaging was performed using a Zeiss Airyscan confocal microscope located at the Biomedical Core Facilities at Kansas State University. Confocal imaging was used for final data acquisition and figure generation to enable optical sectioning. Fluorescent signals corresponding to Alexa Fluor 488, CF®594, and DAPI were visualized using the same settings for all images. Imaging was performed using 20x and 40x objectives. Acquisition parameters were held constant within experiments to permit comparison across samples. Samples were maintained protected from light during handling and imaging to minimize photobleaching.

## Results

To observe the effects of Hippo pathway disruption across developmental stages, RNAi phenotypes of pathway components were analyzed in Tribolium castaneum pupae, larvae, and adults. dsRNA targeting several Hippo pathway genes with well-established mutant phenotypes in Drosophila, including *hippo, warts, salvador, and yorkie*, was generated and used for injection. Primer sequences used for dsRNA synthesis are listed in Table 2.2.2, including two non-overlapping primer sets targeting distinct regions of the *salvador* transcript.

**Table 2.2.2 Primers for Hippo pathway component genes, with T7 promoter denoted in red**

| Gene | Primer Location in Gene | Direction | Sequence (5'–3') |
|---|---|---|---|
| *salvador* | F2 | Forward | **TAATACGACTCACTATAG**GGGAAGGGGTGGTCGGCAAATA |
| *salvador* | R2 | Reverse | **TAATACGACTCACTATAG**GGCCCCAGCGAGTGTCTCAAAT |
| *salvador* | F8 | Forward | **TAATACGACTCACTATAG**GGACCCTTGTCTAGTGCCTTGC |
| *salvador* | R8 | Reverse | **TAATACGACTCACTATAG**GGGCTTATAAAGCCGCGTCAGC |
| *hippo* | F2 | Forward | **TAATACGACTCACTATAG**GGATCGCCACGATTTTGTCCG |
| *hippo* | R2 | Reverse | **TAATACGACTCACTATAG**GATTTCGGGACCATCAAGCGT |
| *warts* | F2 | Forward | **TAATACGACTCACTATAG**GGTATCAGAGCAGTAGCGCGT |
| *warts* | R2 | Reverse | **TAATACGACTCACTATAG**GAGGAGTGGTGTTATTGGCGG |
| *yorkie* | F2 | Forward | **TAATACGACTCACTATAG**GCTCGGACCACAACTTGGGAA |
| *yorkie* | R2 | Reverse | **TAATACGACTCACTATAG**GATTGTCGGGCTTCGTAGTCG |

**Figure 2.1 Control Midgut of Wild Type Adult Beetle**

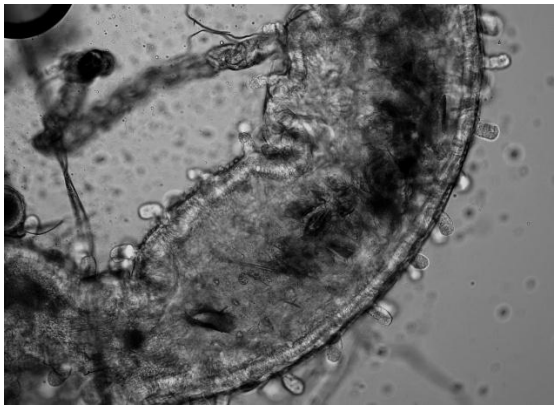

**Figure 2.2 *hippo* dsRNA Injected Midgut**

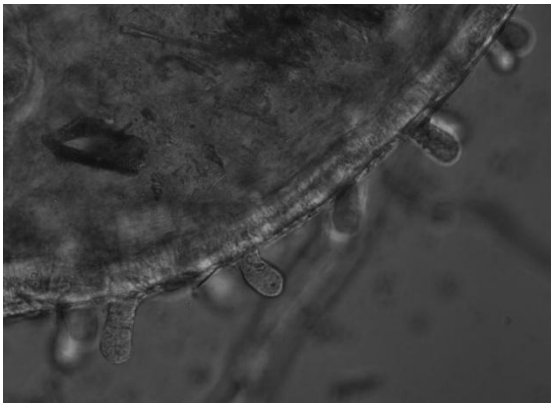

*hippo* dsRNA injected midgut (fully eclosed adult) showing no developmental abnormalities

### *hippo* dsRNA injection in pupae

To assess the role of *hippo* during pupal development, pupae were injected with dsRNA targeting *hippo*. Approximately 6% of injected pupae died within 24 hours post-injection and were classified as injection failures. All remaining individuals completed pupal development and successfully eclosed to adulthood. Adults derived from *hippo*-injected pupae displayed no overt external morphological abnormalities. Dissected adult midguts exhibited normal gross morphology when examined by microscopy. Wild type pupae injected with NF water were dissected and imaged as a baseline for comparison (Fig. 2.1), where stem cell niches (nidi) appear as rounded evaginated structures along the outer edges of the midgut. In *hippo* RNAi

individuals, these stem cell niches were fully evaginated and appeared comparable to those observed in NF water injected controls. No visible disruption of midgut organization was detected (Fig. 2.2). These results indicate that knockdown of *hippo* does not produce detectable morphological changes in the adult midgut under these conditions.

### *warts* dsRNA injection in pupae

To investigate the role of *warts*, pupae were injected with dsRNA targeting this gene. Approximately 4–6% of injected individuals died within 24 hours post-injection and were classified as injection failures. All remaining individuals exhibited complete lethality within 72 hours post-injection. Injected individuals initiated eclosion but failed to complete the process and died during partial emergence from the pupal case (Fig. 2.3, left). Midguts dissected from individuals that progressed sufficiently for tissue isolation displayed gross morphology comparable to controls. Adult midguts exhibited fully evaginated stem cell niches and preserved overall tissue organization in representative images (Fig. 2.3, right). These results indicate that knockdown of *warts* results in lethality during pupal development but does not produce observable midgut morphological defects in individuals that reach late developmental stages.

**Figure 2.3 *warts* dsRNA injected pupae Late-Stage Lethality and Morphology**

Late pupal stage lethality pre complete eclosion in dsRNA *warts* injected pupae (left). Gross morphology comparable to controls in dissected midguts(right).

### *yorkie* dsRNA injection in pupae

Similarly, pupae were injected with dsRNA targeting *yorkie*. Injection resulted in complete lethality within 48 hours post-injection. Approximately 30% of injected individuals died within 24 hours, with the remaining individuals dying by 48 hours (Fig. 2.4, left).

**Figure 2.4 *yorkie* dsRNA injected pupae Early-Stage Lethality and Morphology**

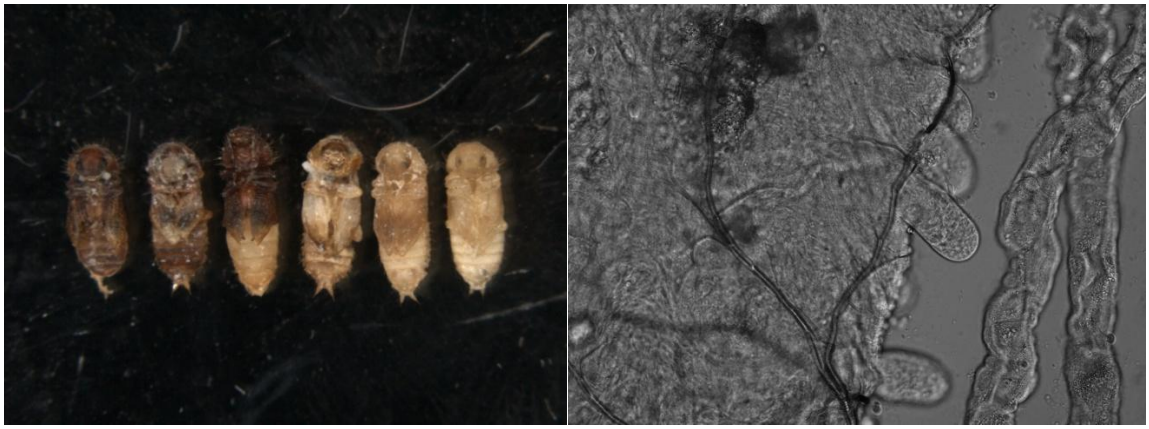

Early pupal stage lethality pre-eclosion in dsRNA *yorkie* injected pupae (left) Midguts dissected displayed comparable morphology to controls (right).

Midguts dissected from injected individuals did not display visible deviations from wild type morphology. Stem cell niches appeared fully evaginated and organized similarly to those observed in *hippo* and *warts* injected groups (Fig. 2.4, right). These results indicate that

knockdown of *yorkie* results in rapid lethality during pupal development but did not produce detectable midgut morphological abnormalities.

### *salvador* dsRNA injection in pupae

Finally, pupae were injected with dsRNA targeting *salvador*. Injection resulted in limited early mortality, with approximately 4–6% of individuals dying within 24 hours post-injection and classified as injection failures. Most injected pupae completed development and successfully eclosed to adulthood. Opposed to other Hippo pathway targets, adult midguts derived from *salvador* injected pupae exhibited pronounced morphological abnormalities. Dissected midguts appeared fragile and frayed (Fig. 2.5, left) compared to wild type (Fig. 2.5, right), and stem cell niches were not evaginated or readily identifiable. Tissue integrity was compromised during dissection, and midguts frequently displayed an expanded and disorganized appearance (Fig. 2.6). These results suggest that *salvador* is required for proper midgut development or maintenance during pupal stages.

**Figure 2.5 *salvador* dsRNA Injected Adult Midgut vs Wild-type Low Mag**

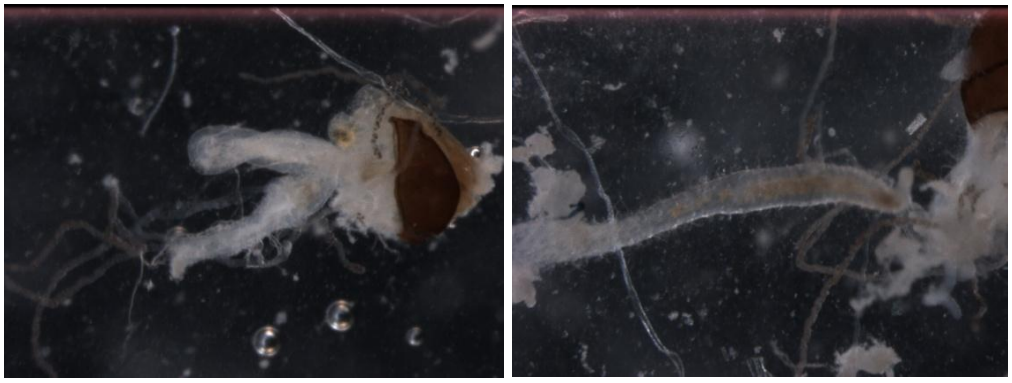

*salvador* dsRNA injected midgut (left) displaying gross abnormalities. Wild type (right) midgut displaying normal morphology.

**Figure 2.6 *salvador* dsRNA Injected Adult Midgut High Mag**

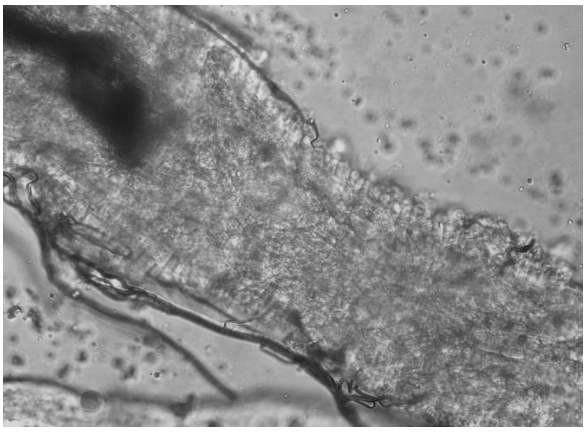

Higher magnification (20x) *salvador* dsRNA injected midgut showing significant changes from wild type. Stem cell niches (nidi) are not readily identifiable.

Complete lethality pre-eclosion was observed following pupal injection of *warts* and *yorkie* dsRNA, while *salvador* knockdown resulted in severe post-eclosion midgut abnormalities. No detectable midgut morphological alterations were observed following *hippo*, *warts*, or *yorkie* knockdown under pupal injection conditions (Table 2.3).

**Table 2.3 Pupal Phenotypes Observed Across 5 Replicate Experiments**

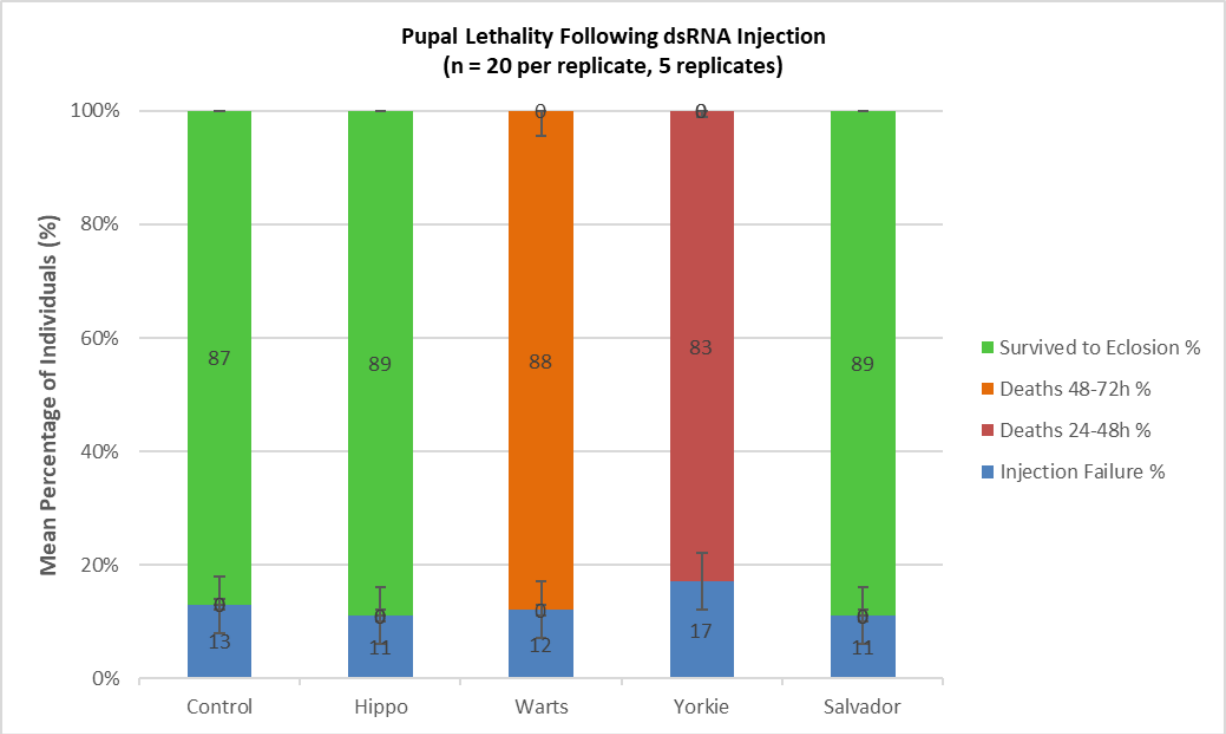


Pupal phenotypes observed across 5 replicate experiments. *salvador* gross morphology alterations were observed in the dissected midguts of fully eclosed adults.

The pronounced midgut phenotype observed following *salvador* knockdown during metamorphosis raised the possibility that these abnormalities were associated with developmental processes occurring during pupation. To evaluate proliferative activity prior to the extensive tissue remodeling associated with metamorphosis, subsequent experiments were performed during the final larval stage (L6), when the midgut contains active stem cell populations that contribute to epithelial maintenance [10]. Larval injections were conducted under conditions consistent with pupal experiments to allow analysis at defined time points (24 and 48 hours) prior to pupation. Proliferative activity within the midgut was assessed using EdU incorporation, with DAPI staining used to visualize total nuclei. Apoptotic activity was evaluated qualitatively in a subset of samples using a TUNEL end-point assay.

## Larval stage injection of Hippo pathway dsRNA

### Control injections, NF water + EdU at 24 hours (+TUNEL at 48 hours), 20x/40x magnification

To establish a baseline for proliferative activity in larval midgut tissue, control larvae were co-injected with NF water and EdU. At 24 hours post-injection, midgut tissues from control larvae displayed discrete EdU-positive nuclei distributed throughout the epithelium at 20× magnification. Labeling appeared sparse, punctuate, and localized, while DAPI staining revealed intact nuclear morphology and preserved epithelial organization (Fig. 2.7). Across five independent biological replicates (n = 20 larvae per replicate), approximately 18–20 larvae per replicate yielded evaluable midgut dissections, and all successfully dissected control midguts displayed this characteristic pattern. These observations establish the baseline pattern of proliferative activity in larval midgut tissue under control conditions.

**Figure 2.7 NF Water + EdU Injected Larval Midgut at 24 Hours**

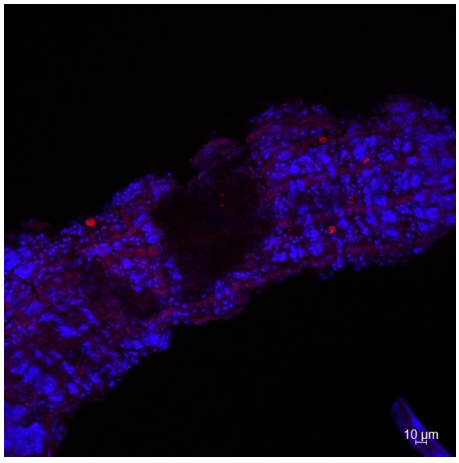


NF Water + EdU injected larval midgut showing preserved structures and localized proliferation nodes as described by literature [10] at 20x magnification.

Control larvae co-injected with NF water and EdU were analyzed at 48 hours post-injection. EdU incorporation remained detectable within the midgut, with the overall distribution of EdU-positive nuclei appearing comparable to that observed at 24 hours in representative images. TUNEL endpoint assay labeling performed at 48 hours revealed detectable signal within the midgut, indicating expected levels of apoptosis. DAPI staining revealed intact nuclear structure and maintained tissue organization. Nidi evagination was not observed at this stage (Fig. 2.8), consistent with previous findings in late larval development prior to pupation [10]. These results indicate that proliferative activity is maintained between 24 and 48 hours in larval midgut tissue under control conditions, with controlled apoptotic activity.

**Figure 2.8 NF Water+ EdU injection at 48 Hours**

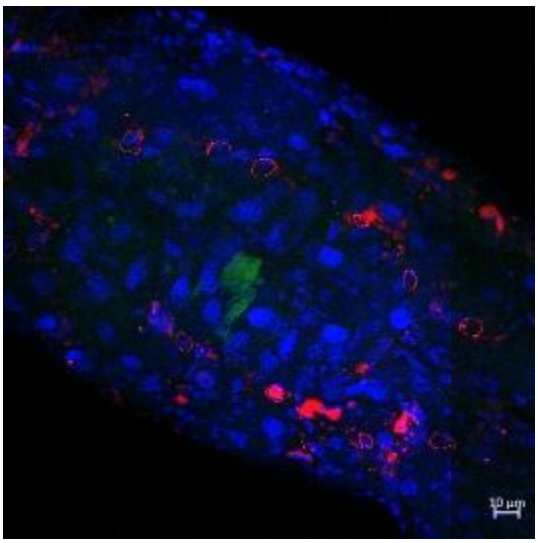

Control sample displaying sporadic apoptotic (TUNEL – Green) and proliferating cells (EdU – Red) at 40x magnification.

### *salvador* dsRNA injection in larvae

Larvae were co-injected with *salvador* dsRNA and EdU to assess changes in proliferative activity and tissue organization within the midgut epithelium. At 24 hours post-injection, DAPI staining revealed nuclei distributed throughout the midgut epithelium (Fig. 2.9), and overall

tissue architecture appeared disrupted. The midgut exhibited an expanded, bloated, and frayed morphology. Widespread EdU incorporation was observed, with EdU-positive signal distributed broadly across the midgut epithelium. Across five independent biological replicates (n = 20 larvae per replicate), approximately 10–12 of 20 larvae per replicate yielded evaluable midgut dissections, of which approximately 6–8 displayed this characteristic proliferative phenotype.

By 48 hours post-injection, dissected midgut tissues exhibited a dense distribution of nuclei throughout the epithelium as revealed by DAPI staining. Nuclear organization appeared irregular, and the midgut remained distended and frayed. Extensive EdU incorporation was observed (Fig. 2.10), with numerous EdU-positive nuclei distributed broadly across the tissue and appearing more widespread than in control samples at the same time point. No detectable TUNEL signal was observed. Across five independent biological replicates (n = 20 larvae per replicate), only approximately 4–5 larvae per replicate yielded evaluable midgut dissections because of progressive tissue fragility, and approximately 3–4 of those specimens displayed the characteristic proliferative phenotype. These results indicate that *salvador* knockdown is associated with sustained proliferative activity, progressive disruption of midgut tissue organization, and increasing tissue fragility during larval development.

**Figure 2.9 *salvador* dsRNA Injected Midgut at 24 Hours**

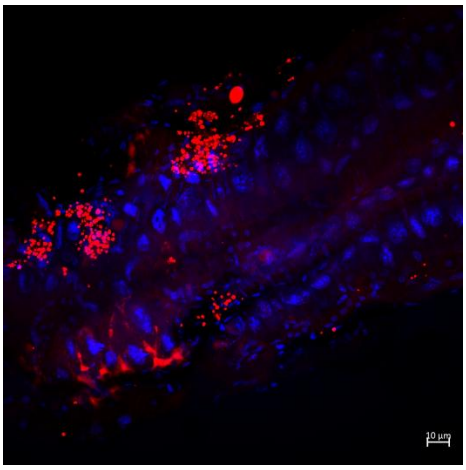

Representative midgut section of *salvador* dsRNA injected insect, showing widespread EdU incorporation.

**Figure 2.10 *salvador* dsRNA Injected Midgut at 48 Hours**

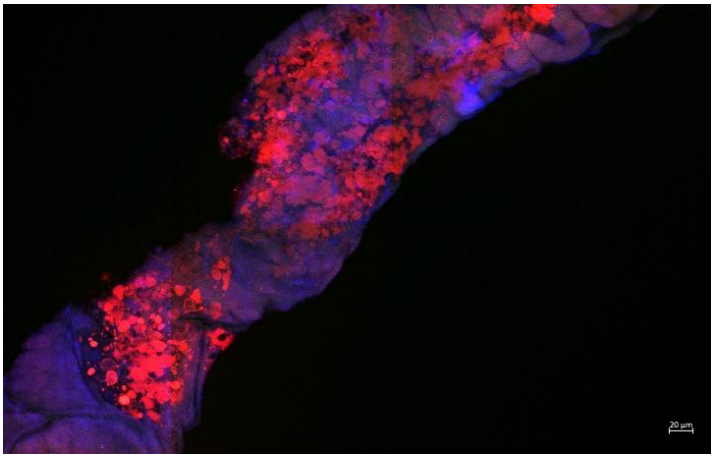

*salvador* dsRNA midgut at 48 hours displaying extensive EdU incorporation diffused throughout the midgut. TUNEL apoptotic signal (green) not detected.

Pronounced midgut alterations were observed following larval injection of *salvador* dsRNA, including reduced tissue integrity and widespread EdU incorporation. Because these observations were made during a developmental stage preceding pupation, the potential contribution of metamorphic remodeling could not be excluded. Adult injections were therefore performed to determine whether similar proliferative abnormalities could also be detected in a

more anatomically stable tissue environment. The adult midgut additionally provided a defined epithelial context in which proliferative changes could be evaluated outside of major developmental restructuring.

## Adult stage injection of Hippo pathway dsRNA

### Control injections, NF water + EdU, at 24 hours post-injection, 20x magnification

A baseline for proliferative activity in adult midgut tissue was developed by co-injecting control adults with NF water and EdU. At 24 hours post-injection, dissected midgut tissues were examined at 20x magnification. DAPI staining revealed normal nuclear spacing throughout the midgut epithelium, and overall tissue architecture appeared intact. Nidi remained clearly identifiable and displayed normal evaginated morphology. (Fig. 2.11). EdU incorporation was limited within the midgut epithelium, with only sparse EdU-positive nuclei detected.

No observable morphological abnormalities were identified.

**Figure 2.11 Adult NF Water + EdU Injections**

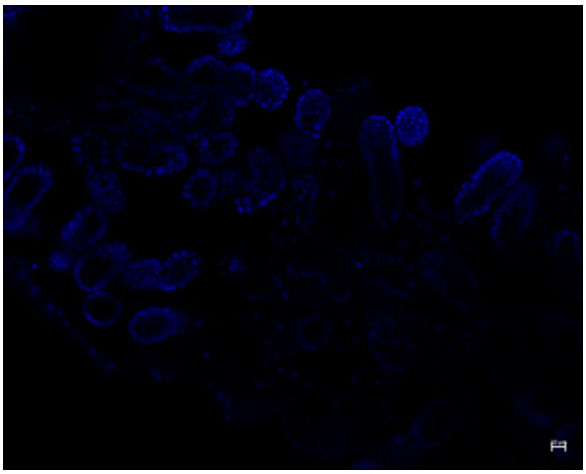

Wild type NF water and EdU co-injection in adult beetles revealing standard morphological characteristics.

**Hippo pathway components (*hippo*, *warts*, *yorkie*) knockdown in adults at 24 hours post-injection (20x magnification)**

Adults were injected with dsRNA targeting either *hippo*, *warts*, or *yorkie* and co-injected with EdU. At 24 hours post-injection, dissected midgut tissues were examined at 20x magnification. DAPI staining revealed evenly distributed nuclei throughout the midgut epithelium, and overall tissue architecture appeared intact in representative images (Figs. 2.12–2.14). EdU incorporation was limited within the midgut epithelium, with only sparse EdU-positive nuclei detected, and labeling appeared comparable to that observed in control adults under identical imaging conditions. No observable morphological abnormalities were identified. These results indicate that knockdown of *hippo*, *warts*, or *yorkie* does not produce detectable changes in proliferative activity or midgut morphology in adult tissue at 24 hours post-injection.

**Figure 2.12 Adult *hippo* dsRNA + EdU Injections**

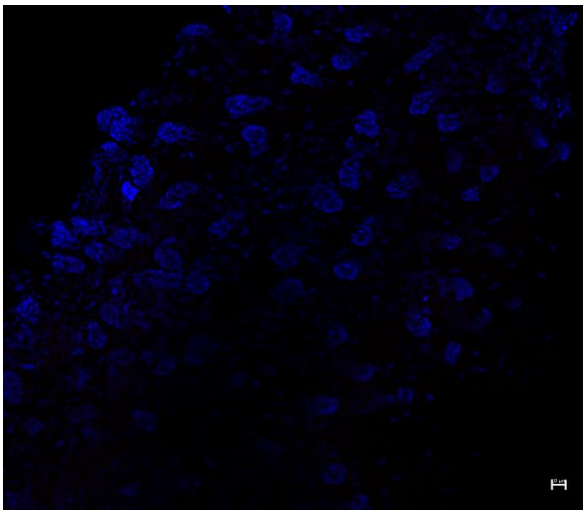

*hippo* dsRNA and EdU co-injected adult with DAPI staining reveals no apparent abnormalities.

**Figure 2.13 Adult *warts* dsRNA + EdU Injections**

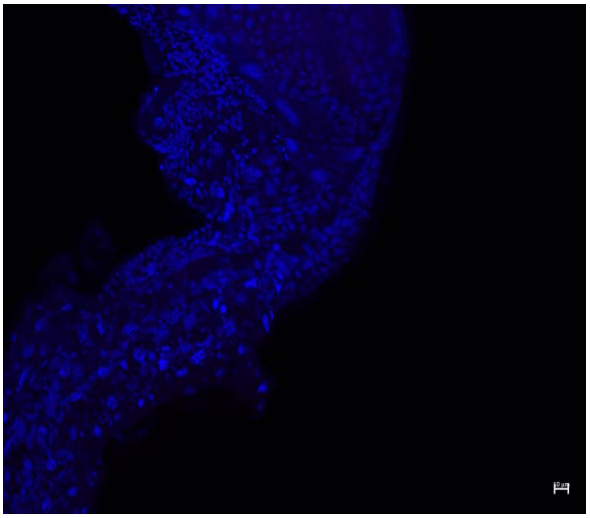

*warts* dsRNA + EdU co-injected adult beetle reveals no apparent morphological abnormalities.

**Figure 2.14 Adult *yorkie* dsRNA + EdU Injections**

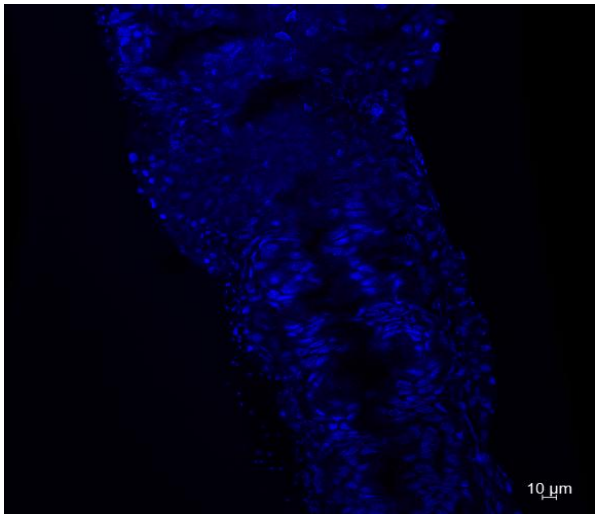


*yorkie* dsRNA + EdU co-injected adult beetle reveals no apparent morphological abnormalities.

### ***salvador* dsRNA injection in adults**

Adults were injected with dsRNA targeting *salvador* and co-injected with EdU to evaluate midgut proliferative responses and associated morphological changes. At 12 hours post-

injection, dissected midgut tissues exhibited relatively preserved tissue integrity, and DAPI staining revealed relatively uniform nuclear distribution (Fig. 2.15). EdU incorporation was detected within the midgut epithelium, with small, localized groupings of EdU-positive nuclei observed that did not extend broadly across the tissue.

By 24 hours post-injection, tissue integrity during dissection was compromised, and DAPI staining revealed irregular nuclear distribution (Fig. 2.16). Extensive EdU incorporation was detected within the midgut epithelium, with large and widespread clusters of EdU-positive nuclei extending across broader regions of the tissue compared to the focal groupings observed at 12 hours. Nuclear crowding was apparent in areas adjacent to EdU clusters, with increased nuclear density observed near regions of elevated EdU incorporation.

At higher magnification (40x), EdU-positive nuclei were arranged in elongated, linear groupings within the epithelium (Fig. 2.17). EdU incorporation appeared dispersed along the midgut, frequently forming string-like patterns (possibly cellular debris) that extended across defined regions of the tissue. Cellular architecture appeared disrupted, with some cell boundaries visibly distorted, and nuclear crowding remained apparent in regions adjacent to areas of elevated EdU incorporation. Examination under brightfield and grayscale imaging revealed reduced tissue integrity and more clearly visualized structural irregularities within the epithelium (Fig. 2.18), with areas of elevated EdU incorporation demonstrating disruption of epithelial integrity and irregular tissue borders.

These results suggest that *salvador* knockdown is associated with progressive increases in proliferative activity and disruption of midgut tissue organization over time.

**Figure 2.15 *salvador* dsRNA+ EdU Adult at 12 Hours**

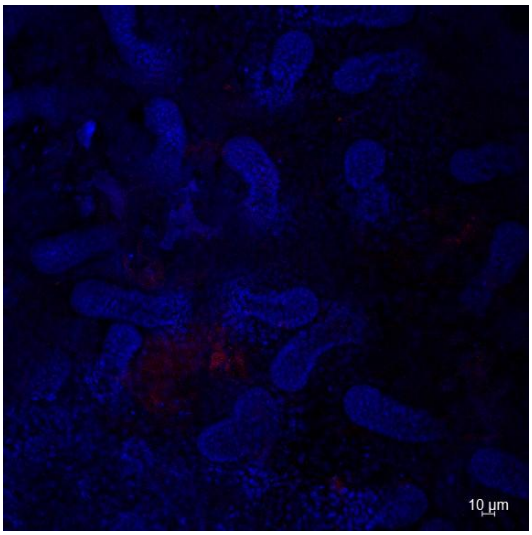


*salvador* dsRNA +EdU co-injected adults dissected at 12 hours post injection reveal localized clusters of EdU incorporation.

**Figure 2.16 *salvador* dsRNA+ EdU Widespread Incorporation at 24 hours**

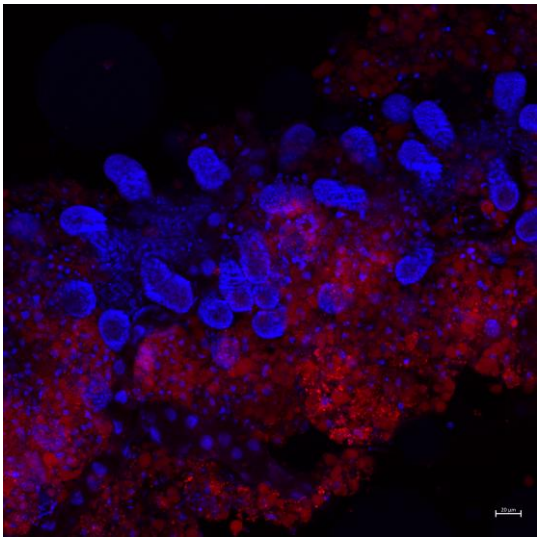

*salvador* dsRNA + EdU co-injection reveals diffuse and widespread EdU incorporation, as well as tissue degradation and deformities to cellular shape.

**Figure 2.17 *salvador* dsRNA+ EdU at 24 Hours 40x Magnification**

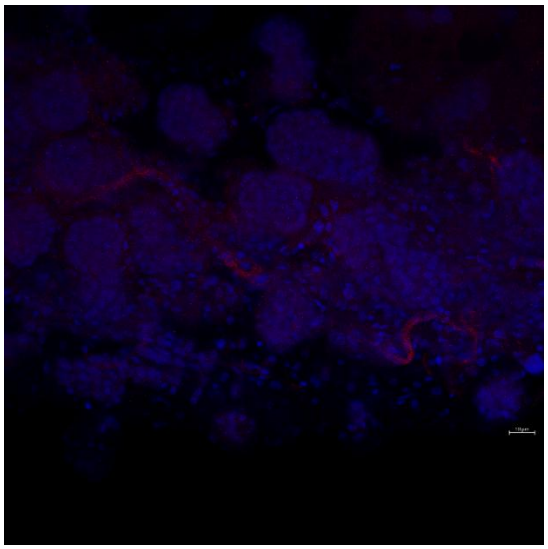

*salvador* dsRNA + EdU co-injection shows string-like formations of EdU incorporation (potentially cellular debris), as well as disrupted cellular organization.

**Figure 2.18 Bright Field Tissue Integrity Observation**

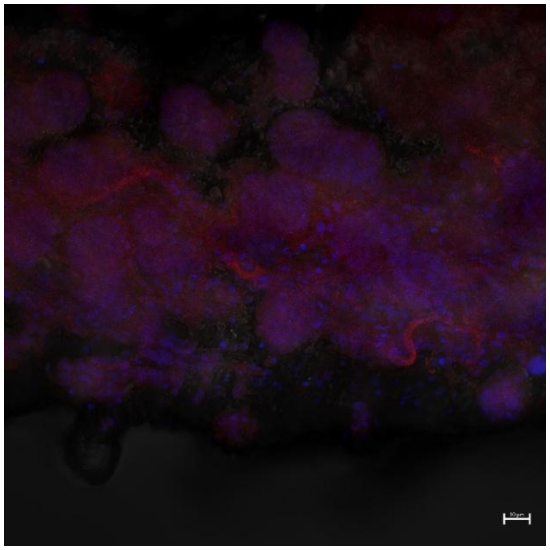

*salvador* dsRNA + EdU co-injection analyzed using additional grayscale/brightfield reveals visible deformities in tissue integrity.

**Independent *salvador* primer validation, 24 hours post-injection, 20x magnification**

Because knockdown of other Hippo pathway components did not produce comparable proliferative phenotypes, the possibility of an off-target effect associated with the initial *salvador* dsRNA construct was considered. To evaluate this possibility, a second non-overlapping dsRNA construct targeting an independent region of the *salvador* transcript was generated and injected under identical experimental conditions. At 24 hours post-injection, dissected midgut tissues displayed phenotypes comparable in severity to those observed with the initial *salvador* dsRNA construct, with increased tissue fragility noted during dissection. Large and widespread clusters of EdU-positive nuclei were observed, and nuclear crowding and disrupted cellular organization were again detected in representative fluorescence images (Fig. 2.19). These results indicate that the observed proliferative and morphological phenotypes are reproducible across independent dsRNA constructs targeting *salvador*.

**Figure 2.19 *salvador* dsRNA+EdU 24 Hours Independent Primer Validation**

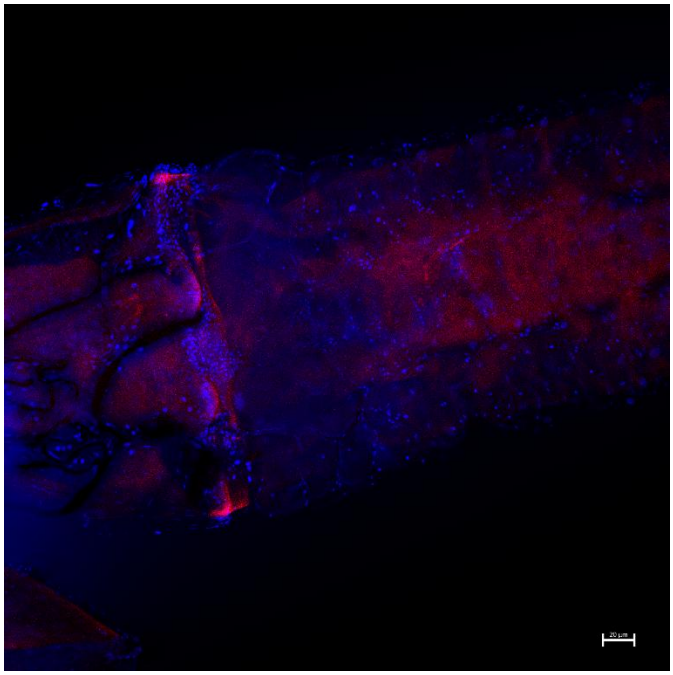

Injection of *salvador* dsRNA +EdU using an independent primer of *salvador* displays equivalent phenotype to previous injections. Midguts were equally frail, and displayed concentrated clusters

of EdU incorporation, opposed to the discrete EdU incorporation nodes observed in control images.

### Formalin fixed paraffin embedded protocol results

Attempts were made to perform formalin-fixed paraffin-embedded (FFPE) sectioning of midgut tissues from both pupal and larval stages for histological analysis. Despite repeated adjustments to fixation, dehydration, and embedding conditions, preservation of tissue integrity suitable for sectioning and imaging was not achieved. Consequently, FFPE-based histological analysis was not included in the final data set.

## Discussion

An initial functional screening of Hippo pathway components was performed during the pupal stage to evaluate pathway contribution during metamorphic remodeling. This developmental stage is characterized by extensive tissue reorganization, cellular turnover, and establishment of adult structures [10]. Differential lethality was observed following knockdown of individual pathway components. Injection of *yorkie* dsRNA resulted in complete mortality within 48 hours, while *warts* knockdown resulted in mortality between 48 and 72 hours. *hippo* knockdown did not produce overt developmental abnormalities beyond injection-associated mortality. *salvador* knockdown permitted survival through pupation but was associated with pronounced adult midgut abnormalities following eclosion, followed by complete mortality within 72 hours post-eclosion.

The differences in lethality and tissue phenotype suggest that disruption of individual pathway components does not produce equivalent developmental outcomes. *yorkie* functions as the primary transcriptional effector of the Hippo pathway, while *warts* acts as an upstream inhibitory kinase regulating *yorkie* activity [6,23]. Severe lethality following *yorkie* and *warts*

knockdown suggests that disruption of core proliferative regulatory activity during metamorphic remodeling is poorly tolerated under these experimental conditions. *salvador* knockdown produced a distinct phenotype characterized by severe disruption of midgut organization rather than immediate developmental failure.

The lethality observed following *yorkie* and *warts* knockdown during the pupal stage is consistent with the established requirement of these pathway components for normal developmental progression in other insect systems [6,23]. *hippo* knockdown during the pupal stage did not result in overt developmental abnormalities beyond injection-associated mortality. Although *hippo* functions as an upstream kinase regulating *yorkie* activity within the pathway [6,23], loss of *hippo* activity in *Drosophila* has more commonly been associated with tissue overgrowth phenotypes rather than developmental arrest [5,18]. The difference in lethality observed between *hippo* and *yorkie* knockdown in *Tribolium castaneum* may reflect differences in pathway position, downstream regulatory effects, or sensitivity to RNAi-mediated disruption under these experimental conditions. These possibilities could be distinguished by measuring knockdown efficiency at matched time points, comparing responses across dsRNA doses, assessing downstream pathway activity, and repeating the experiments with independent non-overlapping dsRNA constructs.

*salvador* knockdown during the pupal stage similarly did not result in immediate lethality comparable to that observed following *yorkie* or *warts* disruption. Individuals survived through pupation and successfully underwent eclosion to adulthood. However, pronounced abnormalities were observed in dissected adult midgut tissues following *salvador* knockdown, including altered tissue morphology and disruption of normal epithelial organization.

The midgut was initially selected for analysis because of the presence of morphologically distinct proliferative structures known as nidi in *Tribolium castaneum* [10]. During metamorphosis, these intestinal stem cell clusters undergo evagination and contribute to remodeling of the adult midgut [10]. Their distinct morphology made disruption of epithelial organization easier to observe after pathway interference.

Following pupal injection of *salvador* dsRNA, abnormalities were observed within the adult midgut upon dissection. Detection of altered midgut morphology in individuals that survived pupation led to further examination of proliferative activity within this tissue during subsequent larval and adult experiments.

Larvae were then examined prior to pupation to determine whether similar abnormalities could be detected before metamorphic remodeling. Late larval development (L6) represents a preparatory stage preceding metamorphosis in which intestinal tissues undergo coordinated changes in proliferation and apoptosis [10]. Examination at this stage made it possible to evaluate pathway disruption before the extensive tissue reorganization associated with pupation.

After *salvador* knockdown in larvae, pronounced alterations in EdU labeling were observed at both 24 and 48 hours post-injection. At 24 hours, extensive EdU incorporation was detected broadly throughout the midgut epithelium compared to controls. Tissue architecture appeared compromised, and the midgut displayed a bloated and frayed morphology upon dissection. Successful isolation of intact midgut tissue was lower compared to control larvae. At 48 hours post-injection, extensive clusters of EdU incorporation remained detectable within the midgut of larvae injected with *salvador* dsRNA.

Previous studies in *D. melanogaster* demonstrated that disruption of Hippo pathway activity alters intestinal stem cell proliferation within the midgut epithelium [18,43,44]. *yorkie*

activation has been associated with increased proliferative activity, while upstream pathway components restrict tissue growth [5,18]. The extensive EdU incorporation observed following *salvador* knockdown in *Tribolium castaneum* resembles proliferative phenotypes previously described following Hippo pathway disruption in *Drosophila*. However, the identity of EdU-positive cells was not determined in the present study.

Adult injections were then performed to determine whether similar abnormalities could also be detected outside of larval developmental remodeling. Adults were examined at defined time points following dsRNA injections to evaluate changes in midgut morphology and EdU incorporation within a more stable tissue environment

In adults, knockdown of *hippo*, *warts*, and *yorkie* did not result in detectable changes in midgut morphology or EdU incorporation relative to controls at the analyzed time point. *salvador* knockdown, however, produced progressively severe abnormalities within the midgut epithelium. At 12 hours post-injection, localized clusters of EdU-positive nuclei were observed. By 24 hours, large and widespread clusters were detected together with compromised tissue integrity, irregular nuclear distribution, and nuclear crowding.

*salvador* has previously been characterized as a scaffold component and tumor suppressor within the Hippo signaling pathway in both vertebrate and invertebrate systems [24,46]. Loss of *salvador* activity has been associated with altered proliferative regulation and tissue overgrowth in multiple experimental models [5,18].

As shown in Figures 2.9,2.10, 2.15, 2.16, 2.17, 2.18 and 2.19, extensive EdU incorporation was observed following *salvador* knockdown in both larval and adult *Tribolium castaneum* midgut tissues. The extent of EdU incorporation observed after *salvador* knockdown resembles proliferative abnormalities previously reported following disruption of Hippo pathway

activity [5,18,23]. However, the identity of proliferating cells observed in the present study was not determined. Although EdU-positive nuclei were frequently observed within or adjacent to morphologically identifiable nidi structures, specific cell type markers were not employed. As a result, the precise cellular populations contributing to the observed EdU incorporation cannot be definitively assigned and remains outside the scope of the present study.

The phenotype observed following *salvador* knockdown was not limited to increased EdU incorporation. Midgut tissues became progressively fragile, difficult to isolate intact, and displayed widespread disruption of normal epithelial organization. Rather than simple expansion of discrete proliferative nidi structures, EdU-positive nuclei became broadly distributed throughout the epithelium. Morphologically identifiable nidi were often difficult to distinguish at later time points, suggesting that normal proliferative organization may have been disrupted rather than uniformly expanded. This pattern may reflect loss of spatial restriction of proliferative activity, disruption of normal differentiation, or structural destabilization of the epithelial tissue following pathway interference. Because specific cell identity markers were not employed, it remains unclear whether the observed phenotype reflects expansion of intestinal stem cells, altered progenitor behavior, failure of normal developmental organization, or a combination of these processes.

Even with these limitations, the severity and reproducibility of the *salvador* phenotype indicate that *Tribolium castaneum* remains useful for identifying strong proliferative and tissue organizational phenotypes following RNAi-mediated pathway disruption. The accessibility of the midgut, together with the efficiency of systemic RNAi in *Tribolium*, provides a practical system for continued investigation of growth regulatory pathways. Further studies incorporating

cell-type-specific markers and additional pathway-level analysis will be necessary to determine the cellular basis of the observed abnormalities.

# Chapter 3 - Molecular analysis of *salvador* expression after RNAi in adult *Tribolium castaneum*

## Introduction

The regulation of tissue growth and cellular proliferation is essential for proper organismal development and independent tissue maintenance. These processes are rigorously controlled by several signaling pathways that coordinate cellular proliferation, stem cell activity, differentiation, and programmed cell death to ensure appropriate tissue size and functionality. Among these pathways, the Hippo signaling pathway plays a central role in regulating proliferation and organ size [3,5].

Regulation of stem cell proliferation is particularly important in epithelial tissues because these tissues undergo continuous cell turnover and depend on resident stem cell populations to maintain tissue integrity and homeostasis [8,9]. In *Tribolium castaneum*, the midgut contains evaginated stem cell clusters known as nidi, which form discrete structures [10]. This organization provides a defined system for examining how perturbation of growth regulatory pathways influences stem cell behavior. To determine whether transcriptional effects of *salvador* knockdown are tissue-specific, gene expression was evaluated across anatomically distinct tissues, including midgut, hindgut, and head. The midgut was selected as the primary tissue of interest due to its defined stem cell populations, while additional tissues were included to distinguish localized effects from broader systemic responses.

Previous analyses demonstrated that RNAi-mediated knockdown of *salvador*, a key regulator of downstream transcriptional effects in the Hippo pathway, in *Tribolium castaneum* produces a reproducible phenotype, gross over proliferation of cells, across multiple life stages, including larvae, pupae, and adults.

While qualitative phenotypic analyses establish functional outcomes, quantitative molecular characterization techniques [TS1.1], such as RNASeq and RT-qPCR, are necessary to explore the transcriptional consequences of this approach.

The Hippo signaling pathway regulates tissue growth in part through transcriptional control of downstream targets such as *yorkie* [5,6]. In *Drosophila*, reduction of Hippo pathway activity, including loss of *salvador*, leads to increased *yorkie* activity and altered expression of genes associated with cell proliferation and survival [5,6]. Similar effects have been observed in mammalian systems, where reduced Hippo pathway activity promotes expression of genes involved in cell cycle progression and inhibition of apoptosis [4,20]. Accordingly, reduction of *salvador* expression is expected to alter downstream transcriptional activity, strengthening the need to define the magnitude and statistical significance of these changes in T. castaneum.

To assess transcriptional changes associated with *salvador* knockdown, RNA sequencing (RNASeq) was performed on RNA isolated 24 hours after RNAi treatment, a time point selected because previous experiments demonstrated a robust proliferative phenotype before extensive tissue disruption became evident. Differential gene expression analysis identified transcripts whose expression differed significantly between *salvador* knockdown and control samples. Gene Ontology enrichment analysis was subsequently performed to identify biological processes and molecular functions associated with the differentially expressed genes. Selected transcripts were independently validated using reverse transcription quantitative PCR (RT-qPCR), which confirmed efficient reduction of *salvador* expression in treated samples.

These approaches enable the examination of transcriptional changes associated with RNAi-mediated reduction of *salvador* and provide molecular context for the phenotypic observations described previously.

## Methods

The *Tribolium castaneum* GA1 (Georgia 1) strain was used for every assay. Statistical significance was established by creating replicate pools (minimum of 3, maximum of 5 pools) containing dissected tissue from 5 individuals.

### Insect rearing

Colonies were maintained under standard conditions that included variable humidity, a temperature of 29 °C, and variable light cycles. Colonies were cultured on organic, pesticide free flour supplemented with 5% yeast.

### Adult selection

Adults were collected as larvae (L6) from a subcultured colony, allowed to complete ecdysis, and injected under the elytra 1–2 days after eclosure to adulthood. No selection was performed to differentiate males from females. Prior to injection, adults were anesthetized by placing them on a mesh receptacle inside a dimethyl ether bottle for 2 minutes 30 seconds.

### Dissections

All tissues were dissected in phosphate buffered saline (PBS) to maintain isotonic conditions and preserve tissue integrity during handling. Dissection in PBS was performed to minimize osmotic stress and to prevent cellular swelling or rupture during tissue isolation. Tissues were maintained submerged in buffer throughout dissection and transfer steps until fixation or downstream processing. Additionally, for tissue-specific RT-qPCR analyses, heads, midguts, and hindguts were pooled by tissue type prior to RNA extraction to obtain sufficient RNA for downstream applications. In addition, pooling provided a representative measure of

average gene expression within each tissue while reducing the influence of biological variation among individual insects.

**dsRNA Synthesis & Validation**

All PCR procedures (except RT-qPCR), gel electrophoresis and nanodrop quantification processes were performed as previously described in Chapter 2.

**dsRNA Injection Conditions and Handling**

dsRNA targeting *salvador* was generated as described in Chapter 2. Adult insects were injected with 100 nL of dsRNA (normalized to 1 nanogram/nanoliter concentration) for the treatment group, 100 nL NF water for the control group. All injection parameters and post injection handling were performed as previously described in Chapter 2. Individuals were collected at 24 hours post injection for molecular downstream analysis. The probe used for RT-qPCR was obtained in the "**QuantiTect SYBR Green PCR Kit**" (200 preparations, Catalog number 204143), purchased from QIAGEN.

**Pooling strategies**

For RNASeq experiments, nine biological replicate pools were generated (three injection control pools injected with nuclease-free water, three untreated negative control pools, and three *salvador* dsRNA treatment pools). Each pool consisted of dissected midguts from five adult beetles. Pooling was performed because individual adult midguts yield insufficient RNA for library preparation and sequencing. In addition, each pool represented the average transcriptional profile of five individuals, reducing the influence of inter-individual biological variation.

For RT-qPCR experiments, three biological replicate pools were generated for each tissue (head, midgut, and hindgut) under each experimental condition (control, housekeeping gene 1, housekeeping gene 2, and *salvador* dsRNA). Heads, midguts, and hindguts were collected from

the same individuals, and each pool contained tissues from five adult beetles. As with the RNASeq experiments, pooling provided sufficient RNA for reliable downstream analyses while allowing each biological replicate to represent the average gene expression of multiple individuals.

**RNA extraction**

Extractions were performed using the "**Direct-zol RNA Microprep Kit**" (200 preparations, Catalog number R2062), purchased from Zymo Research. The kit also contains a DNAse treatment, to ensure no DNA contamination of the RNA. The protocols were followed according to the manufacturer's specifications.

**Reverse transcription of extracted RNA**

Reverse transcription was performed using the "**QuantiTect Reverse Transcription Kit**", purchased from QIAGEN (200 preparations, Catalog number 205313). The protocols were followed according to the manufacturer's specifications.

**Quantification of reverse transcription product**

Products created through Reverse Transcription were quantified using Invitrogen's Qubit 4 fluorometer, with the Invitrogen "**Qubit dsDNA HS assay kit**" (Catalog number 32851). The protocols were followed according to the manufacturer's specifications.

**Equipment for RT-qPCR**

RT-qPCR was performed using **QuantStudio 6 Pro** instrument (and the accompanying Quantstudio6 pro software) from ThermoFisher. The samples were loaded into a 96 well plate and relative quantitative analysis through comparative cycle threshold (CT). The CT value corresponds to the PCR cycle at which fluorescence from amplified product first exceeds the background threshold and is inversely proportional to the initial amount of target nucleic acid.

Relative expression was calculated using the ΔΔCt method according to the manufacturer's recommendations (SYBR Green probe).

**Library preparation & RNA sequencing**

Samples collected were stored at -80 degrees Celsius and subsequently transported to the NGS Core at the College of Veterinary Medicine at Kansas State University. Library preparation was performed at the NGS Core using the "**Total RNA Stranded kit**" **with Ribo-Zero Plus Kit**" (24 preparations, Catalog number 20040526, purchased from Illumina). Sequencing was also performed at the NGS Core, using the **NextSeq2000** platform using the "**P2 Reagents (200 Cycles) kit**" (Catalog number 20077595), purchased from Illumina. All protocols were performed according to the manufacturer's specifications.

**Reference genome**

The reference genome used for downstream analyses and pipeline construction was the current NCBI RefSeq *Tribolium castaneum* assembly, icTriCast1.1 (GCF_031307605.1). This chromosome-level reference assembly comprises 12 assembled chromosomes and associated unplaced scaffolds and was annotated using the NCBI Eukaryotic Genome Annotation Pipeline (Release RS_2024_04), containing 15,518 annotated genes, including 12,172 protein-coding genes, and 22,259 annotated mRNA transcripts. The use of the most recent RefSeq assembly provided an updated and annotated reference for read alignment, transcript quantification, and downstream differential gene expression analyses.

**Computational resources**

Computing was primarily done using the Beowulf HPC cluster at Kansas State University, named **Beocat**. Job submission was primarily handled by **Slurm**. **Galaxy** [41] was used for enrichment analysis.

### RNASeq pipeline

Differential expression analysis was performed using the nf-core/rnaseq pipeline implemented in Nextflow (v3.23.0) [49] (Fig. 3.1). Differential abundance analysis was subsequently conducted using the nf-core/differentialabundance pipeline (v1.5.0) [49] (Fig. 3.2). Raw reads were processed using the default workflow, including quality control, adapter trimming, alignment to the *Tribolium castaneum* reference genome using STAR, and transcript quantification. Differential expression analysis was performed using DESeq2 [50], which applies the Benjamini–Hochberg false discovery rate (FDR) procedure to adjust p-values for multiple hypothesis testing. Pipelines were executed using default settings unless otherwise specified. Detailed QC information can be found in the Supplemental Data 3 – QC.

The analysis was performed using two filtering strategies. The primary analysis applied an adjusted p-value (Benjamini–Hochberg FDR) threshold of 0.05 together with a two-fold change cutoff ($|\log_2 \text{fold change}| \geq 1$). A secondary analysis used only the adjusted p-value (Benjamini–Hochberg FDR) threshold of 0.05 to identify statistically significant transcriptional changes regardless of fold change magnitude.

**Figure 3.1 Nextflow RNASeq Pipeline**

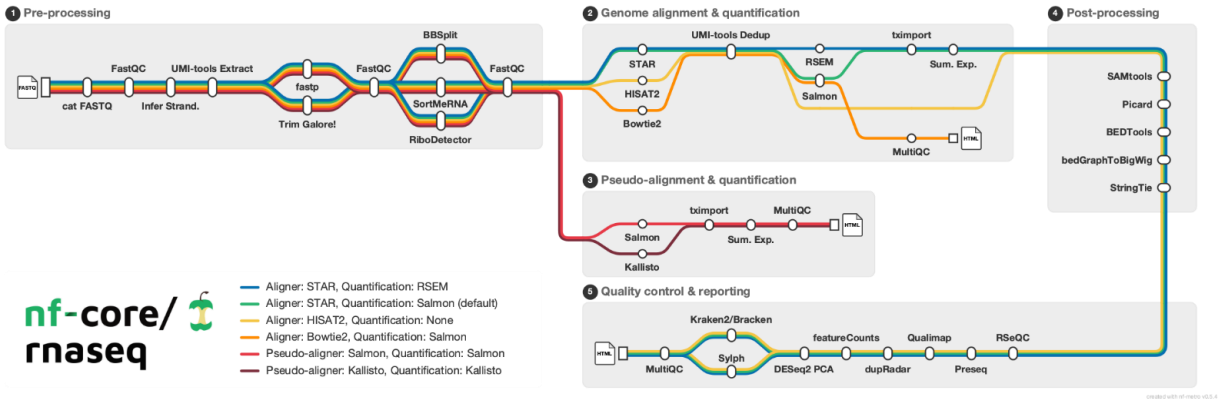

NextFlow RNASeq pipeline, depicting all the tools used to process RNA. For this project, steps 1 through 5 were executed using this model [51].

**Figure 3.2 Differential Abundance Pipeline**

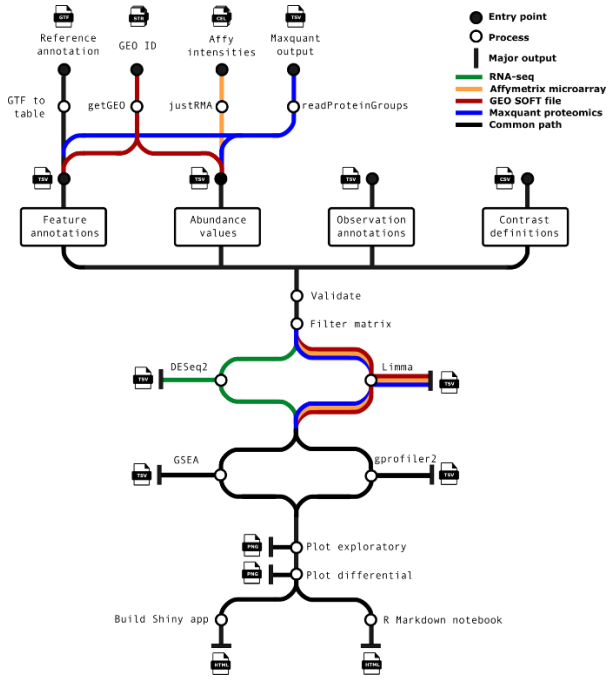


Differential abundance pipeline, used after the RNASeq pipeline to directly observe changes in treatments [51].

## Enrichment analysis

Functional enrichment analysis was performed on the set of genes identified using an adjusted p-value threshold of 0.05 without application of a fold change cutoff, allowing inclusion of all statistically significant transcriptional changes regardless of magnitude. Gene Ontology (GO) annotations were obtained from the NCBI *Tribolium castaneum* icTriCast1.1 (GCF_031307605.1) genome annotation and used to assign differentially expressed genes to biological process, molecular function, and cellular component categories. This approach enabled detection of broader functional patterns that may not be captured under stricter fold change thresholds.

Gene Ontology enrichment analysis was conducted separately for upregulated and downregulated genes across the Biological Process, Molecular Function, and Cellular Component ontologies using the GOEnrichment tool in Galaxy. Overrepresentation of GO terms relative to the annotated background gene set was assessed using a one-tailed Fisher's exact test. P-values were corrected for multiple testing using the Benjamini–Hochberg false discovery rate procedure and GO terms with an adjusted p-value $\leq 0.05$ were considered significantly enriched.

**Statistical analysis and graphic software**

Statistical analysis was conducted in the R (v4.5.1) environment using the car (v3.1-5), lme4 (v1.1-14), and emmeans packages. ΔCt values were used as the response variable, calculated relative to the selected housekeeping genes. R scripts can be found in Supplemental Data 4 – R Scripts.

To account for multiple experimental factors, including treatment, body part, and experiment, a linear model was fitted rather than conducting pairwise comparisons and using the ΔΔCt method. The linear model is appropriate, because it can accommodate a two-way factorial treatment structure to test for interaction effects between body part and treatment and adjust for experiment effects simultaneously, report experimental effects transparently in contrast to the ΔΔCt method, handle any unbalances in the data, and report true 95% confidence intervals adjusting for sample size rather than simple biological variation in raw standard deviations to assess statistical significance[59, 60]. While both methods are similar and the ΔΔCt method does account for mean experimental effects, the linear model is far more transparent and can handle more complex treatment and design structures for proper statistical inference. The initial model included treatment, body part, experiment, and the interaction between treatment and body part.

Pool was initially considered as a random effect; however, the variance associated with pool converged to zero and was therefore excluded from the final model.

Interaction effects were assessed using Type III sums of squares with the Anova function from the car package. As no significant interaction between treatment and body part was detected, the final model included only main effects [60].

Differences between treatment groups were evaluated using estimated marginal means, averaging across levels of body part and experiment. Statistical significance was defined at $\alpha = 0.05$.

The experimental design incorporated multiple sources of variation, including treatment, body part, and experimental run, necessitating a modeling framework that accounted for these factors simultaneously.

Samples were collected in pools, with each pool containing tissues derived from multiple individuals. Pool was therefore initially included as a random intercept to account for potential non-independence among observations. However, the estimated variance associated with this term converged to zero, indicating negligible between-pool variability, and the random effect was excluded from the final model.

Because only two experimental runs were conducted, experiment was included as a fixed effect rather than a random factor. This term accounted for systematic differences between experimental runs, including potential variation in reagents or environmental conditions.

Model assumptions included independence of observations, homoscedasticity of residuals, and normally distributed errors.

**Model structure and statistical considerations**

**Equation 3.1 Full Statistical Equation**

$$y_{ijkl} = experiment_i + bp_j + trt_k + bp \times trt_{jk} + e_{ijkl}$$

Where $Y_{ijkl}$ represents the ΔCT value for observation $l$, corresponding to experiment $i$, body part $j$, and treatment $k$. Treatment ($\mathrm{trt}_k$) consisted of RNAi and control injection groups, body part ($\mathrm{bp}_j$) included head, midgut, and hindgut, and experiment ($\mathrm{exp}_i$) corresponded to the two independent experimental runs. The term $(\mathrm{trt} \times \mathrm{bp})_{jk}$ represents the interaction between treatment and body part.

The residual term $\varepsilon_{ijkl}$ was assumed to be independently and identically distributed with mean zero and constant variance, $\varepsilon_{ijkl} \sim N(0, \sigma^2)$. Observations were treated as independent following removal of the pool effect, as the associated variance converged to zero. Experiment was included as a fixed effect to account for systematic differences between runs, as estimation of a random effect was not supported with only two experimental levels.

Interaction effects were evaluated using Type III sums of squares. As no significant interaction between treatment and body part was detected, a reduced model was used for inference [60]:

**Equation 3.2 Reduced Statistical Equation**

$$y_{ijkl} = experiment_i + bp_j + trt_k + e_{ijkl}$$

**Housekeeping gene selection and primer design for RT-qPCR**

RpS3 and RpL13A were the genes chosen as housekeeping genes, selected based on 2 main criteria: they were stable (no alterations observed) in the RNASeq data and displayed consistently stable behavior in fungal challenges in *Tribolium castaneum* [52].

## Results

To characterize the molecular effects of *salvador* knockdown, transcriptional changes in the midgut were first assessed using RNASeq.

## RNASeq

Given the consistent proliferative phenotype observed following *salvador* knockdown, associated changes in gene expression were assessed using RNASeq. Differential expression was evaluated across control and treatment conditions using an adjusted p-value threshold of 0.05 and a $\log_2$ fold change cutoff of 1.

Principal components analysis based on the 500 most variable genes identified from the whole transcriptome showed that samples grouped broadly by condition, with *salvador* knockdown samples separating clearly from both control groups along the primary component of variance. Replicates within each condition generally clustered together, although increased dispersion was observed among control samples (Graph 3.1).

**Graph 3.1 SAV vs Control Clusters**

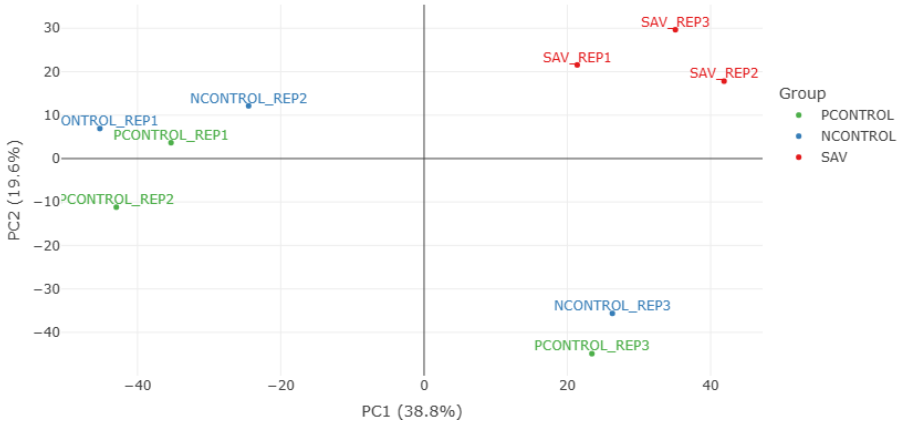


Principal component analysis (PCA) based on the 500 most variable genes identified from the complete transcriptome. *salvador* (SAV) samples clustered separately from the control groups, while PCONTROL_REP3 was identified as an outlier.

To further characterize the transcriptional differences between conditions, differential expression was examined at the gene level. Comparison between the injection control (Pcontrol) and non-injected control (Ncontrol) samples revealed minimal differences in gene expression.

Under the defined significance threshold, no genes were identified as upregulated and three genes were identified as downregulated in this comparison (Graph 3.2).

**Graph 3.2 Stringent Negative Control vs Positive Control**

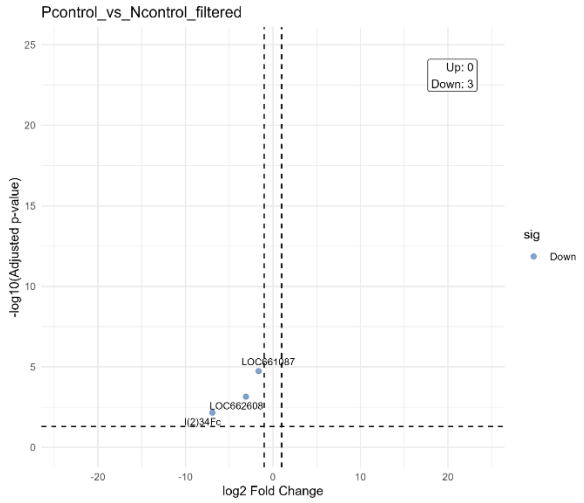


Negative control vs Positive control shows no significant changes in up/down regulation

In contrast, comparison of *salvador* knockdown samples to both control groups revealed clear differences in gene expression. In the comparison between non-injected control (Ncontrol) and *salvador* knockdown samples, 87 genes were identified as upregulated and 18 genes as downregulated (Graph 3.3).

**Graph 3.3 Stringent Negative Control vs SAV**

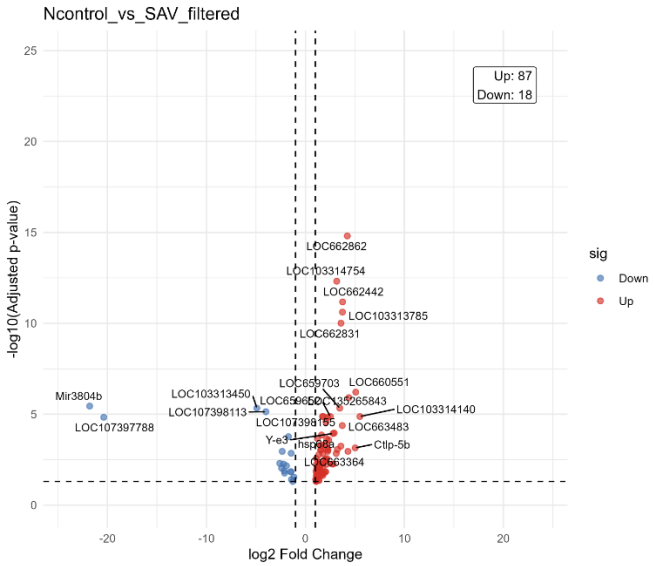


Negative control vs SAV shows significant changes in up and down regulation of gene expression

In the comparison between injection control (Pcontrol) and *salvador* knockdown samples, 252 genes were identified as upregulated and 46 genes as downregulated (Graph 3.4).

**Graph 3.4 Stringent Positive Control vs SAV**

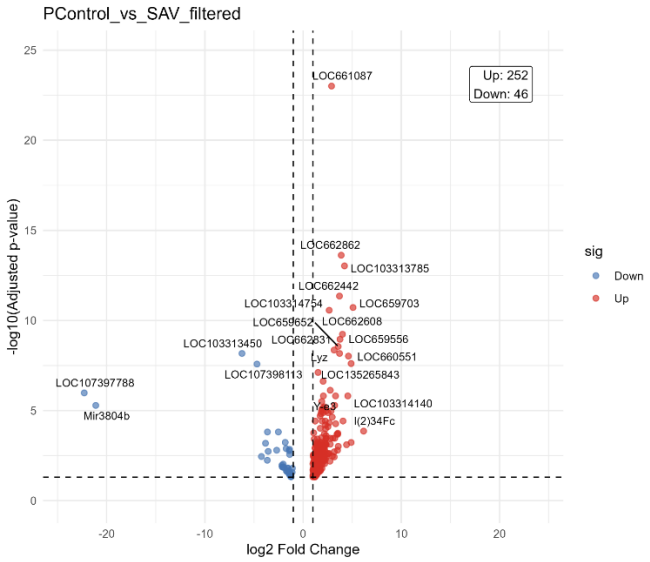


Positive control vs SAV shows similar distribution to Negative control, with clear bias towards upregulated genes.

Across both *salvador* comparisons, the majority of differentially expressed genes were distributed near low to moderate $\log_2$ fold changes, with a smaller subset extending to higher magnitudes, and a clear bias toward upregulated transcripts.

Although injection control (Pcontrol) and non-injected control (Ncontrol) samples did not differ significantly, small differences in expression and variance between groups can lead to different sets of genes being identified in each comparison.

Comparable patterns of differential expression were observed across both control comparisons, indicating that the observed transcriptional changes are associated with *salvador* knockdown rather than the injection procedure.

A limitation of the gene-level interpretation was the extent of predicted or uncharacterized gene annotation in the current *Tribolium castaneum* reference. Several differentially expressed genes were assigned LOC identifiers rather than descriptive gene names, which limited direct functional interpretation at the individual-gene level. Attempts were made to

retrieve corresponding UniProt annotations for these loci to facilitate manual curation; however, annotation coverage was limited and did not substantially improve gene-level identification. For this reason, enrichment analysis was used to evaluate broader functional patterns across the DEG set rather than relying only on named candidate genes.

## Enrichment analysis

### Biological process

Upregulated genes were enriched for processes related to cellular and chemical homeostasis, including intracellular iron ion balance and ion transport, alongside transmembrane and cation transport. Additional terms were associated with muscle contraction and actomyosin structure organization, as well as defense-related processes such as defense response, response to other organisms, and interspecies interaction. Enrichment was also observed for catabolic pathways involving peptidoglycan and aminoglycan metabolism (Figure 1). In contrast, downregulated genes were associated with regulatory processes governing protein phosphorylation and modification, as well as mitotic progression, including the mitotic cell cycle and spindle organization. Protein import was also represented among the enriched terms (Figure 2).

**Figure 3.3 Processes Overrepresented in Upregulated Genes**

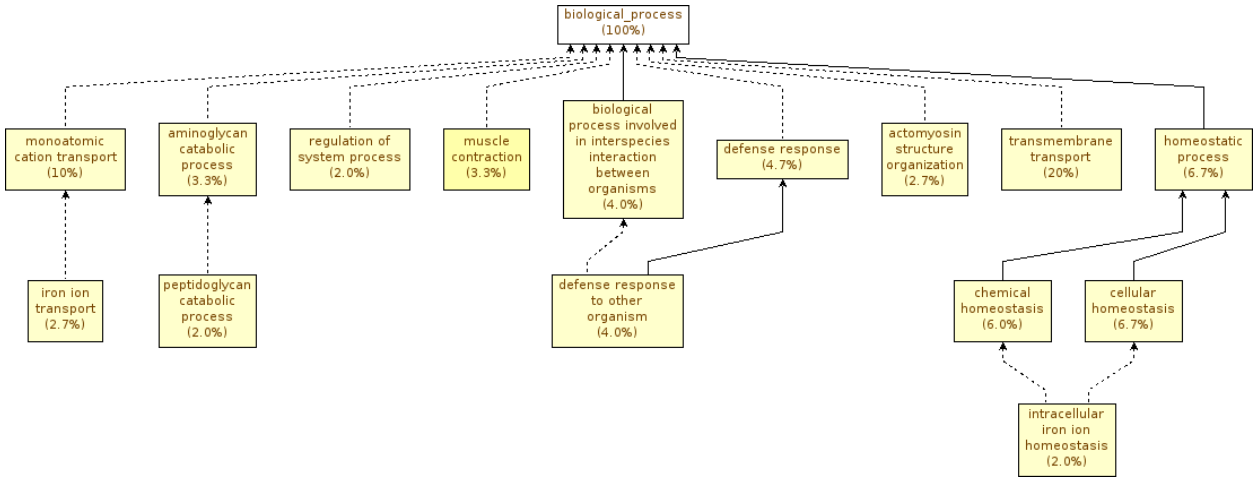

Biological processes overrepresented in upregulated genes.

**Figure 3.4 Processes Overrepresented in Downregulated Genes**

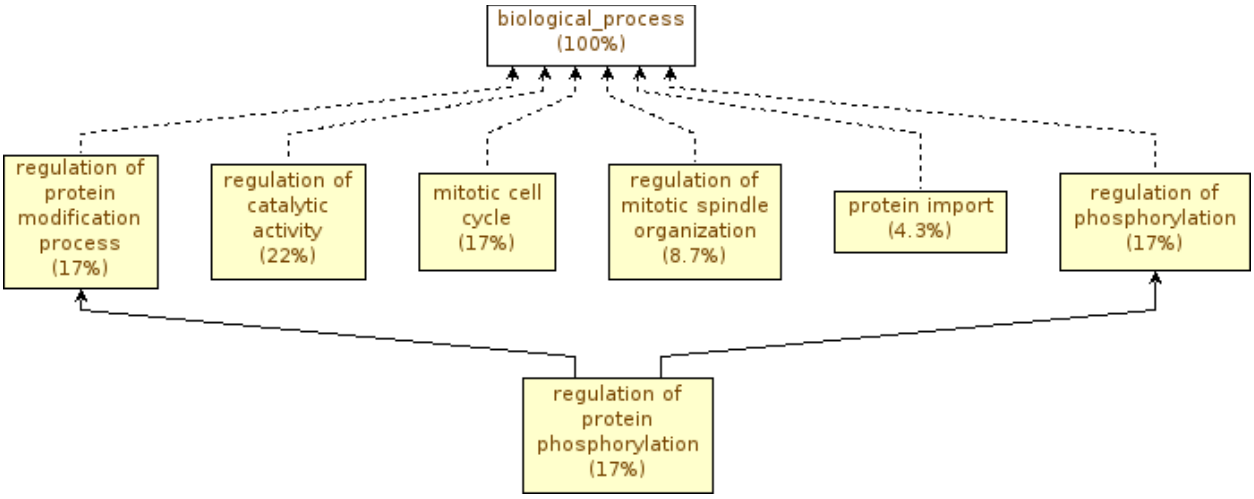


Biological processes overrepresented in downregulated genes.

### Molecular function

A distinct set of functional categories was observed among upregulated genes, dominated by binding activities such as heme, iron ion, and actin binding, together with enzymatic functions including monooxygenase, oxidoreductase, serine-type endopeptidase, and peptidoglycan muralytic activity. Microfilament motor activity was also represented among the enriched terms

(Figure 3). No significant enrichment was detected for downregulated genes under the applied thresholds.

**Figure 3.5 Molecular Processes Overrepresented in Upregulated Genes**

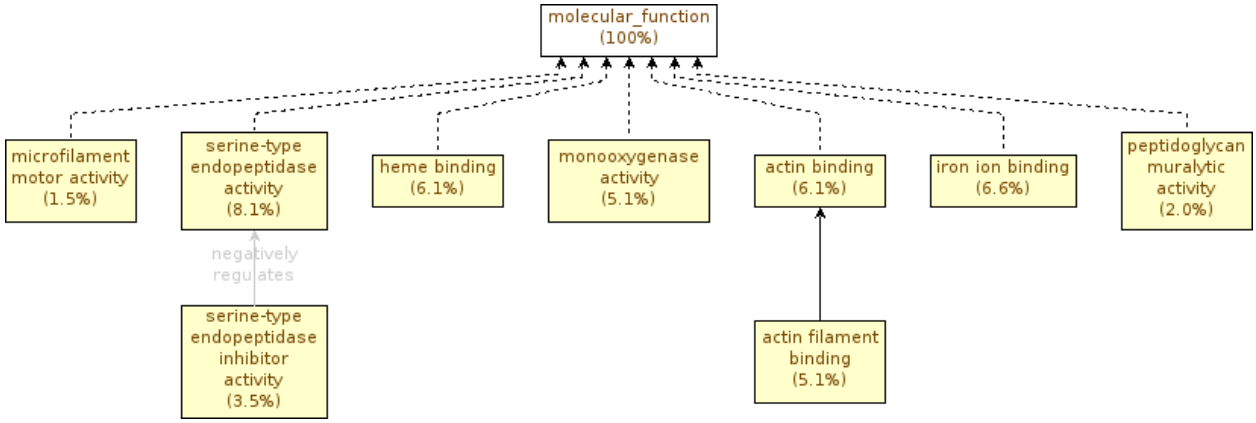


Molecular processes overrepresented in upregulated genes.

### Cellular component

Upregulated genes were primarily associated with extracellular and cell surface localization, including the extracellular region, alongside structural components of the cytoskeleton such as the actin cytoskeleton and supramolecular fiber assemblies. Contractile apparatus associated complexes, including the troponin complex and myosin II complex, were also represented among the enriched terms (Figure 4). No significant enrichment was detected for downregulated genes under the applied thresholds.

**Figure 3.6 Cellular Components Overrepresented in Upregulated Genes**

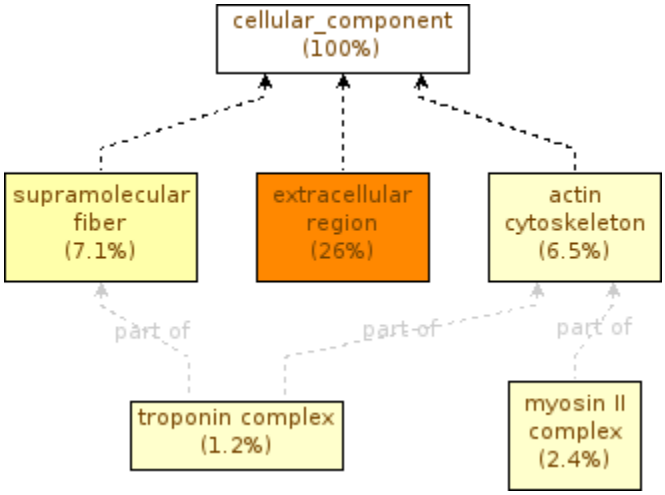


Cellular components overrepresented in upregulated genes.

Analysis using a less stringent threshold (adjusted p-value ≤ 0.05 without application of a fold change cutoff) resulted in an increased number of differentially expressed genes across all comparisons. Visualization of these results using volcano plots showed patterns consistent with those observed under the more stringent criteria, including minimal differences between control groups and a predominance of upregulated genes in *salvador* knockdown samples (Graphs 3.5, 3.6, and 3.7). The expanded gene set was primarily composed of transcripts with lower fold change values, while higher-magnitude outliers remained comparable to those identified under the stricter threshold.

## Graph 3.5 Lenient Positive vs Negative Control

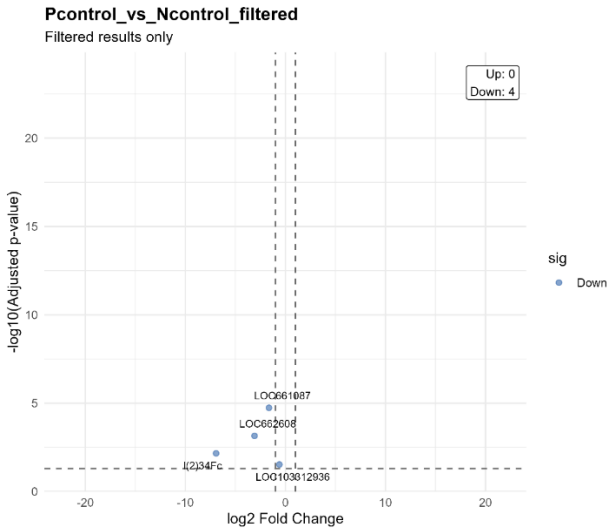


## Graph 3.6 Lenient Negative Control vs SAV

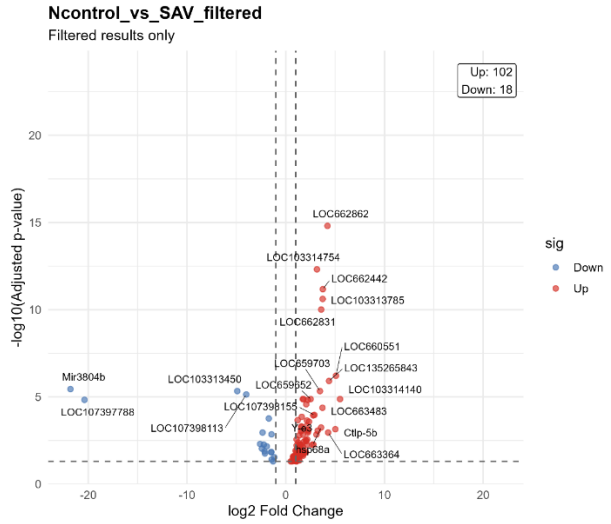

**Graph 3.7 Lenient Positive Control vs SAV**

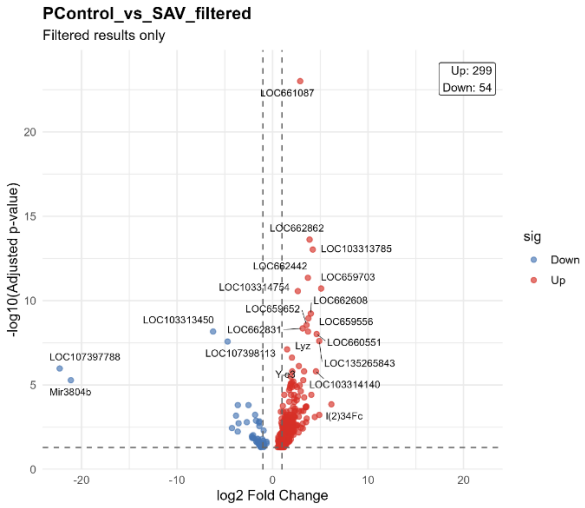


Representation of data with a less stringent cut off method displays additional genes but maintains the same bias and skew of the stricter cut off analysis.

Notably, *salvador* transcript levels were not significantly reduced under the primary analysis criteria, which required both an adjusted p-value ≤ 0.05 and an absolute $\log_2$ fold change ≥ 1. When the fold change criterion was removed, *salvador* met the adjusted p-value threshold (adjusted p-value = 0.0428) but exhibited a modest positive $\log_2$ fold change (0.9911) rather than the expected reduction following RNAi treatment. Consequently, the RNASeq dataset did not independently confirm *salvador* knockdown within the sequenced samples. DESeq2 and processed abundance outputs are provided in Supplementary Data 2.

## RT-qPCR

Quantitative PCR analysis confirmed reduced *salvador* expression following RNAi treatment. This reduction corresponded to an approximate five-fold decrease in relative expression compared to control samples (Graph 3.8). The effect was statistically significant, with an estimated relative expression of 0.21 (95% confidence interval: 0.05–0.79). The confidence interval remained below unity, indicating that the reduction in expression was consistent across

the range of estimated values. Statistical inference using linear models is the recommended approach for complex interactions, to generate p-values, and to generate 95% confidence intervals for inference [59]. Similarly, linear modelling should be conducted on ΔCt values directly and ΔΔCt values can be derived as functions as presented in this analysis and in previous literature [59].

**Graph 3.8 Relative *salvador* Expression After Treatment**

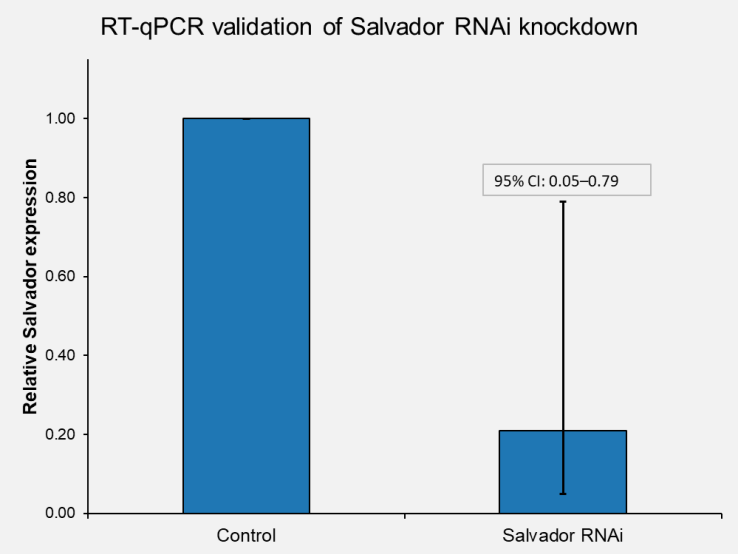


Relative *salvador* expression following RNAi treatment. Expression values are normalized to control samples and presented as relative expression. Error bars represent 95% confidence intervals derived from model estimates, not raw data. The CI range represents the range of relative expression values consistent with our data. While the point estimate suggests roughly a five-fold reduction, the true effect could plausibly be smaller or larger, but remains below control levels

Testing of the full model indicated no evidence for an interaction between treatment and body part (F-test, $p > 0.05$), suggesting that the effect of RNAi treatment on *salvador* expression did not differ across tissues. Consistent with this, no significant differences in expression were detected among body parts (F-test, $p > 0.05$), indicating that *salvador* transcript levels were comparable across head, midgut, and hindgut samples under the conditions tested. In contrast, treatment was identified as a significant main effect (F-test, $p < 0.05$), indicating a consistent mean change in *salvador* expression following RNAi injection across all sampled tissues and experiments. The effect of experiment was also significant (F-test, $p < 0.05$), indicating variation between experimental runs that needed to be accounted for in the model. The estimated mean fold change and 95% confidence interval between treatments, RNAi-WT, was 0.20 [0.05,0.81].

The initial model included a random effect for pool to account for potential non-independence among samples derived from the same group of insects. However, the estimated variance associated with this term converged to zero, indicating minimal variability attributable to pooling. As a result, observations were treated as independent in the final model. Inclusion of experiment as a fixed effect accounted for systematic variation between experimental runs, including potential differences in reagents or environmental conditions.

Because ΔCt values were used as the response variable, differences between treatments reflect relative shifts in amplification cycles rather than absolute expression levels. The observed increase in ΔCt values in RNAi treated samples corresponds to reduced transcript abundance, consistent with delayed amplification relative to control samples. Expression of the selected housekeeping genes remained stable across treatments and tissues, supporting their use for normalization of *salvador* expression.

Melt curve analysis showed single, well-defined peaks for all reactions, indicating absence of primer dimer formation and confirming amplification specificity. Detailed RT-qPCR output, processed expression data and melt curves, is provided in the Supplemental Data 1.

These findings are consistent with the transcriptional patterns observed in the RNASeq analysis, providing independent confirmation of reduced *salvador* expression following RNAi treatment.

## Discussion

*salvador* knockdown in *Tribolium castaneum* results in widespread transcriptional changes that indicate disruption of normal tissue regulation. While increased cellular proliferation was observed phenotypically, the transcriptional profile is characterized by altered

ion transport, cytoskeletal remodeling, and stress-associated pathways, indicating that proliferation occurs within a dysregulated tissue environment.

Comparison between injection control and non-injected control samples revealed minimal differences in gene expression, indicating that the injection procedure itself did not substantially alter transcriptional profiles under the conditions tested. In contrast, *salvador* knockdown was associated with many differentially expressed genes when compared to both control groups, indicating that the observed transcriptional response is driven by *salvador* perturbation rather than the injection process.

Functional enrichment of the upregulated gene set identified terms related to intracellular iron ion homeostasis, ion transport, and transmembrane transport. Cytoskeletal and contractile processes were also represented, including actomyosin structure organization and muscle contraction. Additional enriched terms included defense response, response to other organisms, and interspecies interaction, along with catabolic processes such as peptidoglycan and aminoglycan metabolism. These patterns indicate changes in ion handling, structural organization, and stress or interaction-associated pathways following *salvador* knockdown.

The downregulated gene set was enriched for processes related to regulation of protein phosphorylation and modification, as well as mitotic progression, including the mitotic cell cycle and spindle organization. Terms associated with catalytic regulation and protein import were also represented. These patterns are consistent with reduced activity in pathways linked to cell cycle progression and intracellular regulation following *salvador* knockdown.

In addition to enrichment analysis, several annotated genes within the differentially expressed set align with specific functional categories identified. Lysozyme (Lyz) was strongly upregulated, consistent with enrichment of defense response and response to other organisms.

Idgf2 and Idgf4, which are secreted proteins associated with extracellular remodeling, were also upregulated and correspond to enrichment of cytoskeletal and contractile processes. CYP9Z4, an oxidoreductase, showed increased expression and aligns with enrichment of metabolic activity terms. These gene-level changes do not indicate a direct increase in cell cycle activity but instead point to a perturbed tissue state characterized by stress response, extracellular remodeling, and altered metabolic activity, generally associated with apoptosis.

The downregulation of processes associated with cell cycle progression and intracellular regulation is notable in the context of the proliferative phenotype observed in Chapter 2. *salvador* knockdown was previously associated with increased cellular proliferation, yet the transcriptional profile does not reflect a corresponding increase in traditional cell cycle gene expression. Instead, these results indicate that proliferation occurs alongside a broader disruption of normal regulatory balance, rather than through direct upregulation of cell cycle pathways.

RT-qPCR confirmed reduced *salvador* expression following RNAi treatment, with an estimated five-fold decrease in relative expression compared to control samples. This reduction was consistent across tissues, with no evidence of tissue-specific effects. These results support the effectiveness of the RNAi treatment and provide independent validation of the targeted knockdown.

*salvador* transcript levels were not identified as significantly reduced in the RNASeq dataset under the primary analysis criteria, which required both an adjusted $p$-value $\leq 0.05$ following Benjamini-Hochberg false discovery rate correction and an absolute $\log_2$ fold change $\geq 1$. Under the secondary analysis, which applied only the adjusted $p$-value threshold, *salvador* met the statistical significance criterion (adjusted $p = 0.0428$) but exhibited a modest positive $\log_2$ fold change (0.9911) rather than the reduction expected following successful RNAi.

Consequently, the RNASeq dataset did not independently confirm *salvador* knockdown. Successful *salvador* knockdown within the RNASeq samples could not be independently verified, and interpretations of the transcriptomic response should be considered within that limitation. Several explanations may account for this discrepancy. First, the RNASeq and RT-qPCR experiments were performed using independently generated biological pools and separate RNA extractions. Variation in knockdown efficiency among treatment pools therefore cannot be excluded, and it is possible that *salvador* RNAi was less effective in the samples used for RNA sequencing than in those analyzed by RT-qPCR. Second, the two methods differ substantially in their analytical approaches. RT-qPCR measures transcript abundance for a single target relative to reference genes, whereas RNASeq estimates differential expression across the entire transcriptome using normalized read counts, dispersion estimates, and false discovery rate correction. Finally, because *salvador* expression was not reduced in the RNASeq dataset, interpretations of the transcriptomic response should be made cautiously and should not rely on the assumption that equivalent knockdown was achieved in the sequenced samples.

Although the RNASeq dataset did not independently verify *salvador* knockdown, the reproducible morphological phenotype observed across independent experiments provides a separate line of evidence for biological effects associated with *salvador* RNAi. Consequently, interpretation of tissue organization and proliferative behavior relies primarily on the phenotypic analyses presented in Chapter 2, while the transcriptomic findings provide additional molecular context that should be interpreted within the limitations described above.

Based on the presence of defined stem cell clusters (nidi) in the midgut, *salvador* knockdown was expected to result in localized expansion of these structures, reflecting increased but spatially confined proliferation. Instead, proliferative activity became broadly distributed

throughout the midgut epithelium and was accompanied by progressive disruption of tissue organization and increased tissue fragility. Earlier timepoints revealed more discrete proliferative foci, while later stages showed widespread disruption, indicating progression from localized proliferative activity to widespread tissue disorganization. The transcriptional profile observed at 24 hours post injection did not show enrichment of traditional cell cycle pathways and instead showed increased expression of genes associated with tissue remodeling, ion transport, cytoskeletal organization, and cellular stress. These observations are consistent with widespread proliferative activity occurring alongside disruption of normal tissue organization rather than localized expansion of the nidi.

# Chapter 4 - Discussion: effects of *salvador* knockdown on midgut proliferation and tissue organization

## Overall interpretation of the study

The Hippo signaling pathway is a central regulator of tissue growth, acting to restrict proliferation and maintain proper tissue organization [20,53]. Because *salvador* functions within this broader signaling network with *hippo*, *warts*, and *yorkie*, multiple pathway components were initially evaluated following RNAi treatment [5,6]. Based on previous studies in *Drosophila melanogaster* and mammalian systems, disruption of Hippo pathway activity during development was expected to produce visible abnormalities affecting tissue growth or adult morphology following pupal injection and subsequent adult development [5,6]. Many of the well-characterized *Drosophila* phenotypes arise from imaginal disc overgrowth, particularly in the eye and wing tissues, although comparable structures and developmental dynamics differ in *Tribolium castaneum*. Initial screening was performed during the pupal stage because metamorphosis involves extensive tissue remodeling, cellular turnover, and proliferative activity, making this stage suitable for evaluating potential disruptions in tissue growth and organization. Pupae also provided a technical advantage because their limited mobility allowed more consistent injection and recovery during large-scale phenotypic screening. However, these types of external phenotypes were not consistently observed under the conditions tested. *yorkie* and *warts* knockdown produced lethality during pupation, while *hippo* and *salvador* knockdown did not produce obvious external abnormalities. The absence of clear external phenotypes motivated dissection based examination of internal tissues, particularly the midgut epithelium, which contains organized stem cell populations and undergoes extensive remodeling during

metamorphosis. This tissue therefore provided a useful system for examining how disruption of Hippo pathway signaling affected proliferative organization and tissue architecture.

Initial screening did not produce equivalent outcomes across the four pathway components. *yorkie* and *warts* knockdown resulted primarily in pupal lethality, while *hippo* knockdown did not produce an obvious external or midgut phenotype under the conditions tested. *salvador* knockdown produced the only clear and reproducible midgut abnormality. These differences could reflect distinct biological effects of disrupting individual pathway components, but they could also result from variation in RNAi efficiency, timing, or tthesissue-specific knockdown. Because transcript reduction was not independently confirmed for *hippo*, *warts*, or *yorkie*, the absence of a midgut phenotype in those groups cannot be interpreted as evidence that those genes were successfully reduced without affecting the tissue. Subsequent experiments therefore focused on *salvador*, for which the phenotype could be reproduced, and transcript reduction was later confirmed by RT-qPCR.

The inability to independently verify knockdown efficiency for *hippo*, *warts*, and *yorkie* represents an important limitation of the present study. Because transcript abundance was not measured following RNAi treatment for these genes, the absence of a detectable midgut phenotype cannot distinguish between unsuccessful knockdown, incomplete transcript reduction, insufficient duration of gene silencing, or a genuine biological difference in pathway function. Consequently, these experiments should not be interpreted as demonstrating that *hippo*, *warts*, or *yorkie* lack a role in regulating midgut proliferation or tissue organization. Instead, they served as an initial functional screen that identified *salvador* as the most reproducible candidate for further investigation.

The absence of a detectable phenotype following *hippo* knockdown should therefore be interpreted cautiously. Because *hippo* transcript levels were not independently quantified following RNAi treatment, it is not possible to determine whether the lack of an observable phenotype reflected incomplete knockdown, insufficient RNAi efficiency, temporal limitations of the experimental design, or a true biological difference between *hippo* and the other pathway components. In contrast, *salvador* knockdown was subsequently validated by RT-qPCR and produced a reproducible phenotype using two independent dsRNA constructs, providing greater confidence that the observed tissue abnormalities resulted from reduced *salvador* activity rather than technical variation.

Initial pupal dissections were evaluated using DAPI staining alone. In the *Tribolium castaneum* midgut, stem cell populations are organized into discrete clusters known as nidi, which remain embedded during larval stages and later evaginate from the epithelial surface as the tissue transitions toward the adult configuration [10]. Midguts dissected from *hippo*, *yorkie*, and *warts* knockdown insects did not display obvious structural abnormalities and appeared comparable to wild type controls, including tissues obtained from pupae that had died during development. *salvador* knockdown produced clear abnormalities within the midgut epithelium, where midgut tissues appeared fragile and poorly organized, with disruption of the normal epithelial arrangement and broad distribution of nuclei throughout the tissue rather than the distinct clustered patterns expected in organized nidi structures. However, because EdU incorporation had not yet been implemented, it was not possible to determine whether these observations reflected altered proliferation, apoptosis, tissue degeneration, or disruption of the normal cell death and tissue reorganization processes associated with metamorphosis. To better define the timing and nature of the observed abnormalities, the study was expanded into late

larval (L6) stages prior to completion of metamorphosis. This transition was guided in part by the developmental framework described by Parthasarathy and Palli [10], which identified periods of increased proliferation and tissue restructuring during the larval-to-pupal transition. EdU incorporation studies were performed in L6 larvae and tissues were dissected prior to pupation at 24 and 48 hour timepoints. Both timepoints showed widespread EdU incorporation following *salvador* knockdown. At 24 hours, midgut tissues were enlarged, fragile, and severely disorganized, while at 48 hours tissue integrity was further compromised and tissues frequently fragmented during dissection. Because the 48-hour timepoint corresponds to extensive restructuring of larval tissues during formation of the adult midgut [10], TUNEL assays were incorporated to determine whether the disrupted phenotype was associated with apoptotic fragmentation. However, apoptotic fragments were not detected within *salvador* knockdown tissues under the conditions examined.

Although widespread EdU incorporation was observed in L6 larvae following *salvador* knockdown, interpretation of this phenotype remained complicated by the extensive developmental changes occurring during metamorphosis. At this stage, it remained possible that the observed abnormalities reflected disruption of developmental progression rather than a direct effect on proliferative regulation within the midgut epithelium. To reduce the influence of metamorphic and developmental variables, the study was expanded into adult insects. Midguts dissected 24 hours following injection showed the same widespread EdU incorporation throughout the midgut epithelium observed in larval tissues, along with tissue fragility and disruption of normal organization. Observation of a similar phenotype in adult midguts indicated that the effects associated with *salvador* knockdown were not restricted to tissues actively undergoing metamorphosis or development.

Because the phenotype observed at 24 and 48 hours following *salvador* knockdown was already severe, additional experiments were performed at shorter timepoints to better define when disruption of tissue organization first became apparent. At earlier stages, particularly around 12 hours post injection, EdU-positive cells appeared in more localized regions of the midgut epithelium but not localized within the nidi. By 24 hours, labeling became substantially more widespread and was accompanied by severe disruption of tissue organization. At 48 hours, proliferative labeling remained extensive while tissue integrity became increasingly compromised. This progression from localized proliferative regions to widespread epithelial disruption suggests that the effects of *salvador* reduction extend beyond simple induction of proliferation and involve loss of the spatial organization normally associated with the nidi. Because tissue integrity at 48 hours was severely compromised, subsequent experiments were primarily focused on the 24-hour timepoint. At this stage, the proliferative phenotype was already well established while overall tissue structure remained sufficiently preserved for comparative analysis.

To further evaluate whether the observed phenotype was specifically associated with *salvador* knockdown rather than effects related to a specific dsRNA construct, an independent primer pair targeting a non-overlapping region of *salvador* was generated and used for a second round of dsRNA synthesis and injection experiments. Midguts dissected 24 hours following injection of the independent construct displayed the same widespread EdU incorporation, tissue fragility, and disruption of normal organization observed with the original dsRNA construct. Observation of a comparable phenotype using two independent *salvador* targeting regions supported the reproducibility and specificity of the observed effects.

These observations indicate that the effects of *salvador* knockdown are not limited to increased proliferation but also involve disruption of the spatial organization normally maintained within the midgut epithelium. Under normal conditions, proliferative activity in adults is confined to stem cell populations organized within the nidi, maintaining tissue organization [10]. Following *salvador* reduction, this restriction is lost and proliferative cells become broadly distributed throughout the tissue. This suggests that *salvador* contributes not only to restricting proliferative activity within the midgut, but also to maintaining its confinement within organized regions of the epithelium.

Although the morphological phenotype was reproducible, interpretation of the underlying mechanism required consideration of whether the observed tissue changes reflected a coordinated proliferative response or a broader disruption of epithelial homeostasis. Widespread EdU incorporation suggested increased cell cycle activity within the tissue; however, this observation alone could not determine whether proliferation remained spatially regulated or whether additional cellular processes contributed to the phenotype. Transcriptomic analysis was therefore used to determine whether the morphological changes were accompanied by coordinated activation of canonical proliferative pathways or reflected a more complex tissue response.

Interpretation of the RNASeq data required consideration of several possible explanations. One expectation was that the widespread EdU incorporation and altered tissue organization observed following *salvador* knockdown would be accompanied by enrichment of canonical cell cycle-associated pathways. This was not observed. One possible explanation is that *salvador* RNAi was less effective in the biological samples used for RNASeq, as successful knockdown could not be independently confirmed within that dataset. Alternatively, because

RNASeq was performed using RNA extracted from whole midguts, localized transcriptional changes within proliferating cell populations may have been diluted by surrounding epithelial cells undergoing structural disruption. It is also possible that the transcriptional profile reflects a broader disruption of epithelial homeostasis, in which tissue remodeling, stress responses, and altered cellular organization predominate over classical cell cycle-associated transcriptional programs. The RNASeq findings were therefore interpreted alongside the independently validated RT-qPCR results and the reproducible morphological phenotype rather than as a standalone confirmation of *salvador* knockdown.

Despite the widespread proliferative phenotype, the transcriptional analysis at 24 hours did not show strong enrichment of expected cell cycle-associated pathways. Instead, genes associated with ion transport, cytoskeletal organization, and stress-related processes were upregulated, while pathways linked to mitotic progression were reduced. This transcriptional pattern did not resemble coordinated activation of a canonical proliferative program and instead reflected widespread disruption of tissue organization and normal epithelial structure. Because bulk RNASeq averages transcriptional signal across all sampled cell populations, detection sensitivity for minority proliferative populations may have been reduced [50,54].

RT-qPCR analysis supported reduction of *salvador* transcript levels following RNAi treatment, with an approximate five-fold decrease in relative expression compared to nuclease-free water injected controls across head, midgut, and hindgut tissues. Despite this reduction, strong enrichment of canonical proliferative pathways was not observed in the RNASeq dataset. This difference likely reflects the distinct analytical approaches used by each method. RT-qPCR measures expression of specific target transcripts directly, while bulk RNASeq captures averaged transcriptional signal across heterogeneous cell populations within the tissue. Under these

conditions, localized proliferative populations may contribute strongly to tissue morphology without dominating the overall transcripts detected at the whole tissue level.

Despite the severity of the phenotype at later timepoints, the progression observed across the time-course experiments indicates that the effects of *salvador* knockdown do not reflect immediate nonspecific tissue collapse. Instead, disruption of tissue organization developed progressively alongside increasingly widespread proliferative activity within the midgut epithelium. This progressive phenotype, together with its reproducibility across developmental stages and independent dsRNA constructs, supports the usefulness of the *Tribolium castaneum* midgut as a model for examining how disruption of growth regulatory pathways affects proliferative organization and tissue integrity [33,34].

## RNAi-induced proliferation lacks spatial organization in the midgut

The original aim of this study was to determine whether RNAi could be used to induce proliferation of endogenous stem cell populations within a specific tissue. In the midgut, proliferative activity is normally confined to stem cell populations organized within the nidi [10], and localized expansion of the stem cell compartment was expected following *salvador* knockdown. Instead, proliferative activity became broadly distributed across the epithelium and was associated with progressive disruption of tissue structure rather than localized expansion within defined regions of the midgut. The observed phenotype does not resemble a regulated expansion of the stem cell compartment. Instead, it reflects disruption of the mechanisms that normally confine proliferation to specific regions of the tissue. In epithelial tissues, proliferative activity must remain coordinated with tissue organization to maintain normal structure and function. Under normal conditions, stem cell populations generate new cells within spatially restricted regions while preserving the overall architecture of the epithelium. The widespread

distribution of proliferative cells observed following *salvador* knockdown suggests that this organizational control was disrupted, resulting in proliferation that was no longer confined to defined regions of the tissue.

This distinction is important because increased proliferation alone is not necessarily associated with effective tissue maintenance or regeneration. In regulated epithelial renewal, proliferative activity remains spatially organized and coordinated with differentiation, cell turnover, and preservation of tissue architecture. Following *salvador* knockdown, progressive disruption of epithelial organization, tissue fragility, and loss of the defined proliferative regions normally associated with the nidi were observed. Proliferative activity became increasingly dispersed throughout the tissue rather than remaining confined to specific epithelial regions. Maintenance of spatial restriction therefore appears to be an important component of normal proliferative regulation within the midgut epithelium.

Similar disruption of proliferative organization was observed across larval, pupal, and adult tissues, indicating that the phenotype was not restricted to a single developmental stage or metamorphic context. Observation of widespread proliferative disruption in adult midguts further supports that reduction of *salvador* affects mechanisms involved in maintaining proliferative organization within the midgut epithelium rather than only interfering with developmental remodeling during metamorphosis.

Studies in *Drosophila* have shown that Hippo pathway disruption can promote intestinal stem cell proliferation during tissue regeneration and injury responses [22,27,43]. In these systems, increased proliferative activity is generally described within defined regenerative compartments that preserve overall epithelial organization [8,22]. The phenotype observed following *salvador* knockdown in *Tribolium* differed in that proliferative activity became

broadly distributed throughout the midgut epithelium and was accompanied by progressive disruption of tissue structure. Rather than expansion of a localized regenerative compartment, *salvador* reduction was associated with loss of proliferative restriction across the tissue.

## Identity of proliferating cells in the midgut

EdU labeling identifies cells undergoing DNA synthesis but does not establish cell identity. In the midgut, proliferative activity is normally associated with stem cell populations organized within the nidi [10], suggesting that part of the observed labeling originates from this compartment. However, following *salvador* knockdown, EdU-positive cells are not confined to these structures and instead appear broadly distributed across the epithelium.

Proliferative activity is therefore no longer restricted to the normal stem cell compartment and may involve additional cell populations. These could include progenitor cells, differentiating cells, or cells that would not normally re-enter the cell cycle under steady-state conditions. Without cell type specific markers, these populations cannot be distinguished in the current study. As a result, the identity of the proliferating cells remains unresolved, limiting the ability to determine whether the phenotype reflects expansion of stem cells, recruitment of additional cell types into proliferation, or disruption of normal differentiation within the midgut epithelium.

Identification of the proliferating cell population is important because different cell types would imply substantially different biological interpretations of the phenotype. Expansion of endogenous stem cell populations would suggest altered regulation of normal regenerative compartments, while proliferation of progenitor or differentiating cells could indicate disruption of normal lineage progression within the epithelium. An additional possibility is that differentiated cells may be undergoing inappropriate cell cycle re-entry following *salvador* knockdown. In epithelial tissues, differentiated cells are normally maintained outside the cell

cycle under steady-state conditions, and ectopic re-entry into proliferation is often associated with disruption of tissue homeostasis and epithelial organization. Without cell type specific markers, these possibilities cannot be distinguished in the present study.

In model systems such as *Drosophila*, lineage tracing approaches and cell-type-specific markers allow proliferative responses to be assigned to defined intestinal cell populations [7,8,14]. These tools make it possible to distinguish stem cells from differentiating or mature epithelial populations during regenerative responses and tissue disruption. Comparable lineage tracing approaches and well-characterized intestinal cell-type markers are less extensively developed in *Tribolium*. Incorporation of these approaches into the *Tribolium* midgut system would likely require substantial methodological development beyond the scope of the present study. This limits the ability to determine which epithelial populations contributed to the widespread EdU incorporation observed following *salvador* knockdown, including whether the phenotype reflects expansion of endogenous stem cell populations, altered differentiation dynamics, or broader disruption of epithelial cell-cycle regulation.

## Transcriptional profile following *salvador* knockdown

Despite the widespread proliferative phenotype, the transcriptomic profile at 24 hours does not show enrichment of expected cell cycle pathways. Instead, genes associated with ion transport, cytoskeletal organization, and stress-related processes are upregulated, while pathways linked to mitotic progression are reduced. This pattern does not reflect coordinated cell cycle activation.

The absence of strong enrichment for canonical cell cycle-associated pathways is important because widespread EdU incorporation and extensive tissue disruption might otherwise be expected to coincide with coordinated activation of proliferative transcriptional

programs. Instead, at 24 hours, the observed signatures were dominated by signatures associated with structural remodeling, ion transport, cytoskeletal organization, and cellular stress responses. This suggests that the tissue state following *salvador* knockdown was not characterized by synchronized activation of a proliferative program across the epithelium. Rather, proliferative activity occurred within a tissue environment that was already undergoing substantial structural disruption and loss of normal epithelial organization.

Enrichment of genes associated with ion transport and cytoskeletal organization is also consistent with disruption of normal epithelial structure. In epithelial tissues, cytoskeletal organization contributes to maintenance of cell shape, adhesion, and overall tissue architecture [30]. Ion transport processes are likewise closely associated with epithelial homeostasis and normal tissue function. Alteration of these pathways following *salvador* knockdown is therefore consistent with the extensive tissue fragility and structural disorganization observed morphologically. Rather than reflecting a coordinated proliferative state, the transcriptional profile more closely resembles a tissue undergoing widespread structural disruption and altered epithelial homeostasis.

The use of bulk RNASeq further contributes to this outcome [54]. RNA was isolated from the entire midgut, and the resulting signal represents an average across all cell types within the tissue. If proliferative activity is restricted to a subset of cells, these transcriptional changes may not be detected as enrichment at the tissue level. Similar limitations have been noted in transcriptomic analyses where minority cell populations are diluted within heterogeneous tissues [55].

Differences between RT-qPCR and RNASeq results are also influenced by the distinct analytical approaches used by each method. RT-qPCR directly quantifies predefined target

transcripts with high sensitivity, making it well suited for detection of gene-specific expression changes such as reduction of *salvador* transcript levels following RNAi treatment [50,56]. In contrast, bulk RNASeq measures transcript abundance across the entire tissue simultaneously, producing a composite transcriptomic profile influenced by all cell populations present within the sample [54]. Under these conditions, localized transcriptional changes associated with proliferative subpopulations may contribute strongly to tissue morphology while remaining insufficient to dominate the overall transcriptional profile detected at the whole-tissue level. This distinction is particularly important in disrupted tissues where heterogeneous cellular responses may occur simultaneously within the same epithelial environment.

## Technical constraints and future directions

The results of this study establish a reproducible phenotype following *salvador* knockdown, characterized by widespread proliferation and loss of spatial organization in the midgut. Interpretation of this response is limited by the resolution of the approaches used, particularly the inability to distinguish between cell types and relate transcriptional changes to their spatial context. The following sections address these limitations and outline approaches that would improve characterization of this phenotype.

## Resolution of cell identity and spatial expression

Interpretation of the proliferative response is limited by the lack of resolution at the level of individual cell types and spatial organization within the midgut. EdU labeling identifies cells undergoing DNA synthesis but does not distinguish between stem cells, progenitor cells, or differentiating cells. At the same time, bulk RNASeq provides a single averaged profile across the entire tissue [54]. This loss of spatial resolution is particularly important in the context of the phenotype observed following *salvador* knockdown. The central characteristic of the phenotype

was not simply increased proliferation, but loss of the normal spatial restriction of proliferative activity within the midgut epithelium. Because bulk RNASeq averages transcriptional signal across the entire tissue, localized expression differences associated with discrete proliferative regions cannot be separated from the surrounding epithelial environment. As a result, transcriptional changes occurring within restricted proliferative populations may become obscured within the larger tissue-level expression profile. Consequently, it is not possible to determine which cell populations are contributing to the observed transcriptional changes or how these changes relate to the spatial distribution of proliferative activity.

This limitation is directly relevant to the central observation of this study. Proliferation following *salvador* knockdown is no longer confined to discrete regions of the midgut, yet the transcriptional data cannot resolve whether this reflects expansion of the stem cell compartment, recruitment of additional cell types into proliferation, or disruption of normal differentiation processes. These possibilities cannot be distinguished with the approaches used here.

Approaches that preserve spatial context would substantially improve interpretation of this phenotype. Spatial transcriptomic methods could resolve whether transcriptional changes remain associated with discrete proliferative regions or become broadly distributed throughout the epithelium following *salvador* knockdown [55]. This distinction is biologically important because the phenotype observed in the present study was defined not only by increased proliferation, but also by loss of the normal spatial restriction that characterizes proliferative organization within the midgut. Spatially resolved approaches would therefore allow direct comparison between proliferative localization, tissue organization, and regional transcriptional responses within the same tissue environment. In parallel, the use of cell type specific markers and co-labeling strategies would allow direct identification of the proliferating population.

Interpretation of the transcriptional response is also constrained at the level of gene annotation. A substantial proportion of differentially expressed genes lacked functional characterization, restricting the depth of enrichment analysis and limiting the ability to define the pathways contributing to the observed phenotype [33,47]. As a result, the RNASeq profile can be described generally, but not fully resolved in terms of specific molecular mechanisms.

## Technical constraints in *Tribolium castaneum*

Several technical aspects of this study required adaptation of existing methods for use in *Tribolium castaneum*. Protocols for EdU labeling are well established in mammalian systems and have also been applied in insect models, though experimental approaches differ substantially between systems [10]. In this study, EdU delivery was achieved through direct injection, requiring adjustment of injection conditions to maintain viability while achieving sufficient labeling. While effective, this approach introduces variability in label distribution and uptake within the tissue.

Additional constraints arise from the limited availability of reagents for *Tribolium* [33,34]. The lack of established antibodies and validated cell-type markers restricts analysis to transcriptional and morphological approaches. Protein-level validation of *salvador* knockdown was not feasible within the timeframe of this study, and the development of species-specific antibodies would require substantial time and validation. Similarly, the absence of well-defined markers for midgut cell populations limits the ability to assign identity to proliferating cells or to track changes in differentiation state.

These constraints do not prevent identification of the phenotype described here, but they limit the level of resolution at which the underlying cellular and molecular processes can be

defined. Continued development of tools specific to *Tribolium castaneum* would improve the ability to link proliferative activity, gene expression, and tissue organization within this system.

## Model considerations for regeneration studies

*Tribolium castaneum* provides several advantages for RNAi-based studies, particularly the strong systemic RNAi response observed following dsRNA injection [36,38,42]. Unlike *Drosophila*, where many RNAi approaches rely on tissue-specific transgenic systems, RNAi in *Tribolium* can produce broad organism-wide knockdown following direct dsRNA delivery [38,42]. This allows rapid evaluation of gene function across developmental stages and tissue contexts without generation of complex transgenic lines. In the present study, this systemic response enabled efficient induction of *salvador* knockdown and reproducible identification of proliferative abnormalities within the midgut epithelium, while also allowing comparison of phenotypic effects across multiple tissues and developmental contexts.

However, the ability to extend these findings toward controlled, tissue-specific regeneration is limited by practical constraints inherent to this system. The small size of the organism and its tissues restrict spatial resolution, limit the amount of material available for analysis, and complicate repeated or localized sampling. Larger vertebrate systems allow more precise spatial manipulation and recovery of defined tissue regions, which are important advantages for regeneration-focused studies. In addition, the lack of well-defined cell type markers and established tools for targeted manipulation within specific regions of adult tissues limits the ability to precisely control and monitor proliferative responses.

Studies focused on controlled induction of proliferation and regeneration within defined tissue compartments require precise spatial manipulation and high-resolution analysis of proliferative responses [1,11,13]. Increased tissue accessibility allows more precise spatial

delivery of reagents, improved recovery of localized tissue regions, and higher-resolution analysis of proliferative responses. These features are particularly important when attempting to distinguish between localized stem cell expansion, transient regenerative responses, and widespread disruption of tissue organization. Greater tissue volume also facilitates integration of spatial transcriptomics, lineage tracing, and repeated sampling approaches that are difficult to implement in smaller invertebrate systems.

Within this context, *Tribolium castaneum* remains highly valuable for identification of strong proliferative phenotypes following RNAi-mediated disruption of growth regulatory pathways. The efficiency of systemic RNAi, together with the ability to evaluate phenotypes across developmental stages and tissue environments, makes this system well suited for rapid functional analysis of candidate regulatory genes. Larger insect systems may provide advantages for tissue dissection, imaging resolution, and spatial characterization because of increased organ size and easier tissue handling. Species such as Manduca sexta have historically been useful for physiological and developmental studies for this reason. At the same time, many larger insect models lack the degree of systemic RNAi efficiency and experimental throughput available in *Tribolium*. The phenotype observed following *salvador* knockdown demonstrates that *Tribolium* can effectively identify disruptions in proliferative organization and tissue architecture, while complementary systems may be

better suited for resolving fine spatial and cellular mechanisms underlying regenerative control.

## Conclusion

This study demonstrates that RNAi-mediated reduction of *salvador* in *Tribolium castaneum* induces a strong proliferative response within the midgut, with RT-qPCR confirming

a clear reduction in *salvador* transcript abundance. However, proliferative activity did not remain confined to the spatially restricted regions normally associated with organized stem cell populations. Instead, proliferation became broadly distributed throughout the epithelium and was accompanied by progressive disruption of tissue structure and loss of normal tissue organization across developmental stages and timepoints examined. Transcriptional analysis further demonstrated that this phenotype was not associated with coordinated enrichment of canonical proliferative pathways, but rather with signatures consistent with structural disruption and altered epithelial homeostasis. Interpretation of the findings presented here should be considered in the context of several experimental limitations. Functional comparison among Hippo pathway components was limited because knockdown efficiency was independently validated only for *salvador*. In addition, EdU incorporation identified cells undergoing DNA synthesis but did not establish the identity of the proliferating cell population. Interpretation of the transcriptomic response was further constrained because RNASeq did not independently confirm *salvador* knockdown within the sequenced samples, bulk RNASeq lacked spatial and cell-type resolution, and many differentially expressed genes remain poorly characterized in *Tribolium castaneum*. These limitations do not alter the reproducibility of the observed phenotype but define important directions for future investigation.

Induction of proliferation through disruption of growth regulatory pathways does not necessarily produce controlled or tissue-compatible growth. Following *salvador* knockdown, proliferative activity became uncoupled from the spatial and structural constraints that normally maintain epithelial organization within the midgut. This distinction is particularly important in the context of regenerative biology, where successful tissue maintenance depends not only on induction of cell division, but also on preservation of spatial regulation, tissue architecture, and

coordinated cellular organization. The phenotype observed in this study highlights the importance of growth regulatory mechanisms in maintaining the balance between proliferation and functional tissue organization. More broadly, these findings establish *Tribolium castaneum* as a useful system for studying how disruption of growth control alters proliferative organization within epithelial tissues.

# Bibliography

1. Hoang, D. M., Pham, P. T., Bach, T. Q., et al. (2022). Stem cell-based therapy for human diseases. Signal Transduction and Targeted Therapy, 7, 272.

2. Hwang, N. S., Varghese, S., & Elisseeff, J. (2007). Controlled differentiation of stem cells. Early Human Development, 83(4), 255–262.

3. Broder, M. S., Quock, T. P., Chang, E., et al. (2017). The cost of hematopoietic stem-cell transplantation in the United States. American Health & Drug Benefits, 10(7), 366–373.

4. Zheng, Y., & Pan, D. (2019). The Hippo signaling pathway in development and disease. Developmental Cell, 50(3), 264–282.

5. Zhao, B., Tumaneng, K., & Guan, K. L. (2011). The Hippo pathway in organ size control, tissue regeneration and stem cell self-renewal. Nature Cell Biology, 13(8), 877–883.

6. Huang, J., Wu, S., Barrera, J., et al. (2005). The Hippo signaling pathway coordinately regulates cell proliferation and apoptosis by inactivating *yorkie*, the Drosophila homolog of YAP. Cell, 122(3), 421–434.

7. Micchelli, C. A., & Perrimon, N. (2005). Evidence that stem cells reside in the adult Drosophila midgut epithelium. Nature, 439(7075), 475–479.

8. Jiang, H., & Edgar, B. A. (2011). Intestinal stem cells in the adult Drosophila midgut. Experimental Cell Research, 317(19), 2780–2788.

9. Fre, S. (2015). Intestinal stem cells. Stem Cell Biology and Regenerative Medicine, 12, 455–475.

10. Parthasarathy, R., & Palli, S. R. (2008). Proliferation and differentiation of intestinal stem cells during metamorphosis of the red flour beetle, Tribolium castaneum. Developmental Dynamics, 237(4), 893–908.

11. Zhu, H., Yu, B., & Yang, L. (2018). Exogenous and endogenous stem cells for skeletal regeneration. Stem Cells International, 2018, 1–9.

12. Corley, L. S., & Lavine, M. D. (2006). A review of insect stem cell types. Seminars in Cell & Developmental Biology, 17(4), 510–517.

13. Wei, J., Baptista-Hon, D., Wang, Z., et al. (2023). Bioengineered human tissue regeneration and repair using endogenous stem cells. Cell Reports Medicine, 4(8), 101156.

14. Zeng, X., Chauhan, C., & Hou, S. X. (2013). Stem cells in the Drosophila digestive system. Advances in Experimental Medicine and Biology, 786, 63–78.

15. Gao, Y., Feng, B., Han, S., et al. (2019). Role of TGF-β/Smad pathway in the transcription of pancreas-specific genes during beta cell differentiation. *Frontiers in Cell and Developmental Biology, 7*, 351

16. Kim, W., & Jho, E. H. (2018). The history and regulatory mechanism of the Hippo pathway. BMB Reports, 51(3), 106–118.

17. Ikmi, A., Gaertner, B., Seidel, C., et al. (2014). Molecular evolution of the *Yap*/*yorkie* proto-oncogene and elucidation of its core transcriptional program. Molecular Biology and Evolution, 31(6), 1375–1390.

18. Xiao, Y., & Dong, J. (2021). The Hippo signaling pathway in cancer: A cell cycle perspective. Cancers, 13(24), 6212.

19. Anders, R. A., Valero, V., III, & Pawlik, T. M. (2015). Emerging role of Hippo signaling and YAP in hepatocellular carcinoma. Journal of Hepatocellular Carcinoma, 2, 69–79.

20. Mo, J. S., Park, H. W., & Guan, K. L. (2014). The Hippo signaling pathway in stem cell biology and cancer. EMBO Reports, 15(6), 642–656.

21. Ben-David, U., Gan, Q. F., Golan-Lev, T., et al. (2014). Selective elimination of human pluripotent stem cells by an oleate synthesis inhibitor discovered in a high-throughput screen. *Cell Stem Cell, 12*(2), 167–179.

22. Jiang, H., Tian, A., & Jiang, J. (2016). Intestinal stem cell response to injury: Lessons from Drosophila. Cellular and Molecular Life Sciences, 73(17), 3337–3349.

23. Tapon, N., Harvey, K. F., Bell, D. W., et al. (2002). *salvador* promotes both cell cycle exit and apoptosis in Drosophila and is mutated in human cancer cell lines. Cell, 110(4), 467–478.

24. Snigdha K, Gangwani KS, Lapalikar GV, et al. (2019). Hippo signaling in cancer: Lessons from Drosophila models. *Frontiers in Cell and Developmental Biology, 7*, 85

25. Zhu, H., Zhou, Z., Wang, D., et al. (2013). Hippo pathway genes developed varied exon numbers and coevolved functional domains in metazoans for species-specific growth control. BMC Evolutionary Biology, 13, 76.

26. Ravisankar, P., Lai, Y. T., Sambrani, N., et al. (2016). Comparative developmental analysis of Drosophila and Tribolium reveals conserved and diverged roles of abrupt in insect wing evolution. Developmental Biology, 409(2), 518–529.

27. Staley, B. K., & Irvine, K. D. (2010). *warts* and *yorkie* mediate intestinal regeneration by influencing stem cell proliferation. Current Biology, 20(17), 1580–1587.

28. Bando, T., Mito, T., Maeda, Y., et al. (2009). Regulation of leg size and shape by the Dachsous/Fat signaling pathway during regeneration. Development, 136(13), 2235–2245.

29. Liu, S., Zhang, P., Song, H., et al. (2016). *yorkie* facilitates organ growth and metamorphosis in Bombyx mori. International Journal of Biological Sciences, 12(8), 917–930.

30. Schroeder, M. C., & Halder, G. (2012). Regulation of the Hippo pathway by cell architecture and mechanical signals. Seminars in Cell & Developmental Biology, 23(7), 803–811.

31. Pantalacci, S., Tapon, N., & Léopold, P. (2003). The *salvador* partner *hippo* promotes apoptosis and cell-cycle exit in Drosophila. Nature Cell Biology, 5(10), 921–927.

32. Donninger, H., Allen, N., Henson, A., et al. (2011). *salvador* protein is a tumor suppressor effector of RASSF1A with Hippo pathway-independent functions. Journal of Biological Chemistry, 286(21), 18483–18491.

33. Richards, S., Gibbs, R. A., Weinstock, G. M., et al. (2008). The genome of the model beetle and pest Tribolium castaneum. Nature, 452(7190), 949–955.

34. Pointer, M. D., Gage, M. J. G., & Spurgin, L. G. (2021). Tribolium beetles as a model system in evolution and ecology. Heredity, 126(6), 869–883.

35. Vommaro, M. L., Donato, S., Caputo, S., et al. (2024). Anatomical changes of Tenebrio molitor and Tribolium castaneum during complete metamorphosis. Cell and Tissue Research, 396(1), 19–40.

36. Miller, S. C., Miyata, K., Brown, S. J., et al. (2012). Dissecting systemic RNA interference in the red flour beetle Tribolium castaneum: Parameters affecting the efficiency of RNAi. PLoS ONE, 7(10), e47431.

37. Cao, M., Gatehouse, J. A., & Fitches, E. C. (2018). A systematic study of RNAi effects and dsRNA stability in *Tribolium castaneum* and *Acyrthosiphon pisum* following injection and ingestion of analogous dsRNAs. International Journal of Molecular Sciences, 19(4), 1079.

38. Tomoyasu, Y., & Denell, R. E. (2004). Larval RNAi in Tribolium (Coleoptera) for analyzing adult development. Development Genes and Evolution, 214(11), 575–578.

39. Ulrich, J., Dao, V. A., Majumdar, U., et al. (2015). Large-scale RNAi screen in Tribolium reveals novel target genes for pest control and the proteasome as prime target. BMC Genomics, 16, 674.

40. Afgan, E., Baker, D., Batut, B., et al. (2018). The Galaxy platform for accessible, reproducible and collaborative biomedical analyses. Nucleic Acids Research, 46(W1), W537–W544.

41. Sebio, A., & Lenz, H. J. (2015). Molecular pathways: Hippo signaling, a critical tumor suppressor pathway. Clinical Cancer Research, 21(22), 5002–5007.

42. Linz, D. M., Clark-Hachtel, C. M., Borràs-Castells, F., et al. (2014). Larval RNA interference in the red flour beetle, Tribolium castaneum. Journal of Visualized Experiments, 92, e52059.

43. Karpowicz, P., Perez, J., & Perrimon, N. (2010). The Hippo tumor suppressor pathway regulates intestinal stem cell regeneration. Development, 137(24), 4135–4145.

44. Ren, F., Wang, B., Yue, T., et al. (2010). Hippo signaling regulates Drosophila intestinal stem cell proliferation through multiple pathways. Proceedings of the National Academy of Sciences of the United States of America, 107(49), 21064–21069.

45. Seo, Y., Park, S. Y., Kim, H. S., et al. (2020). The Hippo-YAP signaling pathway as a guardian of intestinal stem cells. Biomedicines, 8(12), 554.

46. Bucher, G., Scholten, J., & Klingler, M. (2002). Parental RNAi in Tribolium castaneum (Coleoptera). *Current Biology, 12*(3), R85–R86.

47. NCBI Resource Coordinators. (2024). Database resources of the National Center for Biotechnology Information. Nucleic Acids Research, 52(D1), D10–D17.

48. Park, Y. (2023). *[Unpublished Tribolium laboratory reference material]*. Department of Entomology, Kansas State University.

49. Di Tommaso, P., Chatzou, M., Floden, E. W., et al. (2017). Nextflow enables reproducible computational workflows. Nature Biotechnology, 35(4), 316–319.

50. Love, M. I., Huber, W., & Anders, S. (2014). Moderated estimation of fold change and dispersion for RNASeq data with DESeq2. Genome Biology, 15(12), 550.

51. Patel, H., Manning, J., Ewels, P., et al. (2026). *nf-core/rnaseq: nf-core/rnaseq v3.26.0 - Chromium Cuttlefish (3.26.0)* [Data set]. Zenodo.

52. Lord, J. C., Hartzer, K., Toutges, M., et al. (2010). Evaluation of quantitative PCR reference genes for gene expression studies in *Tribolium castaneum* after fungal challenge. *Journal of Microbiological Methods, 80*(2), 219–221.

53. Boopathy, G. T. K., & Hong, W. (2019). Role of Hippo pathway-*YAP/TAZ* signaling in angiogenesis. Frontiers in Cell and Developmental Biology, 7, 49.

54. Wang, Z., Gerstein, M., & Snyder, M. (2009). RNASeq: A revolutionary tool for transcriptomics. Nature Reviews Genetics, 10(1), 57–63.

55. Rao, A., Barkley, D., França, G. S., et al. (2021). Exploring tissue architecture using spatial transcriptomics. Nature, 596(7871), 211–220.

56. Anders, S., & Huber, W. (2010). Differential expression analysis for sequence count data. Genome Biology, 11, R106.

57. Zhai, J., Li, W., Liu, X., et al. (2023). Tiny Drosophila intestinal stem cells, big power. Cell Biology International, 47(1), 3–14.

58. Liu, Q., Pan, S., Liu, S., et al. (2021). Suppressing Hippo signaling in the stem cell niche promotes skeletal muscle regeneration. Stem Cells, 39(6), 737–749.

59. Yuan, J. S., Reed, A., Chen, F., & Stewart, C. N., Jr. (2006). Statistical analysis of real-time PCR data. BMC Bioinformatics, 7, 85.

60. Milliken, G. A., & Johnson, D. E. (2009). Analysis of Messy Data, Volume 1: Designed Experiments (2nd ed.). CRC Press.